Natural Hazards (2026) 122:193
https://doi.org/10.1007/s11069-025-07963-0

ORIGINAL PAPER

Landslides impact and management on human settlements over 3000 years: the case of the Montilla Castle Hill (Córdoba, Spain)

Francisco J. Jiménez-Espejo[1] · Lourdes González-Castillo[2] · Francisco Lamas[3] · Francisco José Martínez-Moreno[4] · Jesús Galindo-Zaldívar[2,5] · Jon Camuera[6] · Sergio Moyano[7] · José A. Peláez[8] · José Luis Urbano[7] · Mónica Camacho Calderón[9] · Raimundo Ortiz[10]

Received: 5 August 2025 / Accepted: 27 December 2025

Abstract
In recent decades, global urbanisation has increased dramatically. The study of urbanised areas over the last millennium offers valuable insight into the long-term landslide hazards associated with human settlements. Anthropogenic environmental impact and urbanisation in southern Iberia began around 2200 yr BCE, rendering this region a unique location to examine interactions between building construction and landslide over millennial timescales. The Montilla Castle Hill, in south Spain, was selected for this study due to its clear evidence of landslides and confirmed historical occupation dating back to the Copper Age. This study adopted a multidisciplinary approach, integrating archaeology, geology, geophysics, geotechnical modelling and related disciplines to characterize construction types and pathologies, as well as landslide ages, critical stability threshold values, landslide mechanisms and key features. The obtained data were compared with regional paleoclimate records and earthquakes/tsunamic events in south Iberia. Four landslide activity phases have been dated: from 650–550 BCE, from 400 to 200 BCE, from 1400 to 1450 and along the XVIII to XX centuries. Observations revealed that the presence of major buildings at the summit of the Castle Hill, at the landslide crown, were a key factor in promoting the reactivation of ancient landslides. This study found no evidence linking climate conditions with slope stability, but a correlation with major regional earthquakes was observed, in agreement with the modelled values obtained.

Keywords Historic landslides · Electrical resistivity tomography · Geotechnical modelling · Archaeology · South Iberia · Montilla

Extended author information available on the last page of the article

Published online: 20 February 2026

1 Introduction

Present day global warming together with population increase and distribution is contributing to a higher risk to landslides (e.g., Haque et al. 2019; Svennevig et al. 2024). Landslide is a down slope movement of soil or rock, which occurs due to local geological and groundwater conditions, extreme weather events, earthquakes and other factors (Highland and Bobrowsky, 2008). The study of the interaction of past and present landslides with human settlements around the world is useful in order to reduce this source of risk (Gariano and Guzzetti 2016). The Iberian Peninsula has been continuously inhabited by genus Homo from the last 1.2 Myr (Carbonell et al. 2008) making this region a key location for studying human and environment interactions. In southern Iberia, the earliest evidence of significant human-induced landscaped dated back to Copper/Bronze Age, around 2200 yr BCE (Carrion et al. 2007; Jimenez-Espejo et al., 2024). During recent decades, the interest for past coastal earthquakes and tsunamis impact in human societies has also increased in this region (Luque et al. 2001; Lario et al. 2011; Álvarez-Martí-Aguilar and Machuca Prieto, 2022a). However, few studies have focused on the long-term impact of landslide stability in human activities or how past societies resolved technological problems associated to landslide reactivations. The long-term presence of anthropogenic constructions in southern Iberia offers a unique opportunity to study slope dynamics over millennial timescales.

Geophysical approaches, especially electrical methods, are increasingly being applied to landslide characterization because they provide non-invasive spatial information in heterogeneous subsurface environments that can be difficult to characterise using surface observations or intrusive sampling (Merritt et al. 2018; Whiteley et al. 2019). Electrical methods constitute a useful tool to analyse the evolution of subsurface moisture distribution affecting landslide active or passive surfaces, as well as to identify spatial and temporal variations of geological (Martínez-Moreno et al. 2013, 2017, 2018; Uhlemann et al. 2017; Martos-Rosillo et al. 2019; Whiteley et al. 2021) and archaeological features (Noel and Xu 1991; Papadopoulos et al. 2009; Milo et al. 2022).

The Montilla Castle Hill (Córdoba, Spain; Figs. 1, 2, 3) was occupy by a fortress (*Castillo* in Spanish) that was mostly demolished and the building on its summit is now a monumental granary. This is a great location for exploring the interaction between past and present societies with landslides, as archaeological evidences indicates continuous human occupation and construction from at least from the Bronze Age (3500 to ~ 2200 yr BCE) to date (Bermúdez et al., 2000), and trace of major landslides can be recognized in the surface along the archaeological sequence (Fig. 4). Despite landslide's impact on both, the hill's topography and the castle –as well as older structures– no detailed study on the stability and evolution of this slope has yet been complete. This study aimed to highlight how archaeological records integrated with a multidisciplinary approach can provide unique information for slope dynamics reconstruction of the Montilla Castle Hill and contribute to the knowledge of landslide occurrence through time and space, mandatory for a better landslide risk comprehension (Sassa et al. 2017). To characterize the subsurface structure and the geometry of the landslide, as well as to reconstruct its impact on various constructions, several methods were employed, including 2D electrical resistivity tomography (ERT), geotechnical modelling, seismology, archaeology and historical accounts.

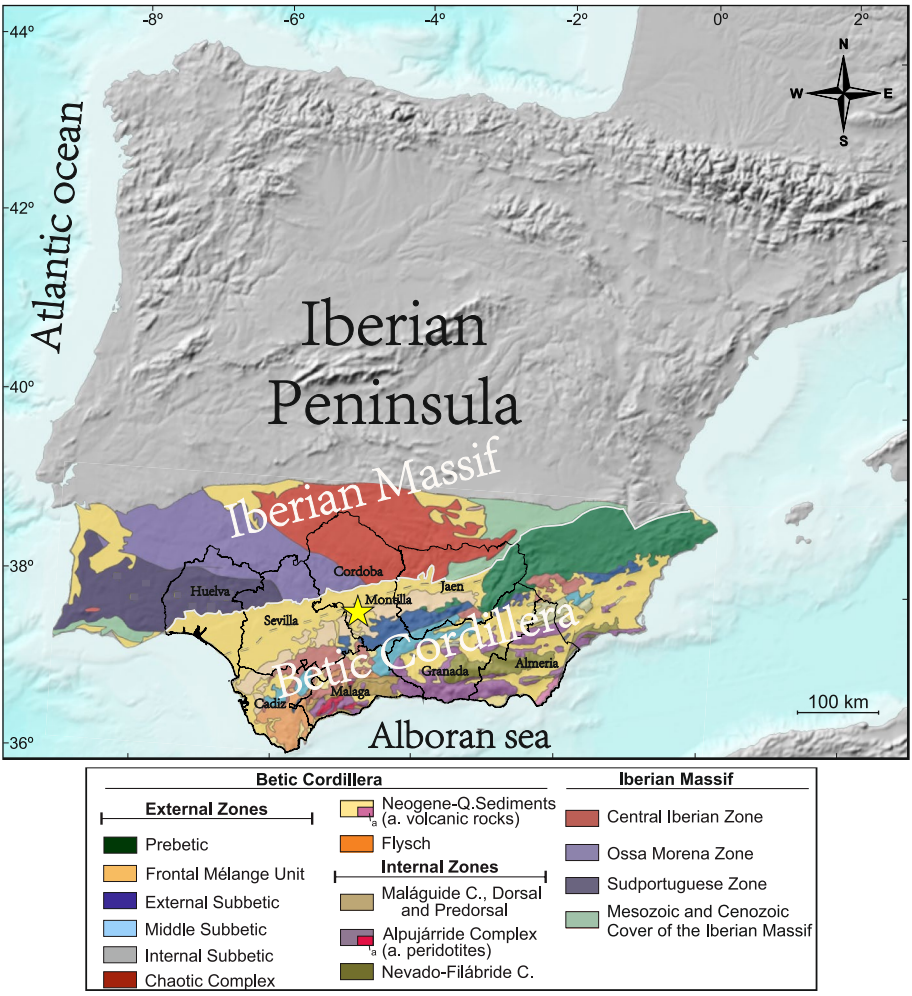

Fig. 1 Geological map of the study area in the Betic Cordillera. The location of Montilla is indicated with a yellow star

2 Montilla castle hill setting

2.1 Historical and archaeological setting

At the Castle Hill, anthropogenic deposits with variable thickness and different epochs are also present. Five previous archaeological campaigns (Bermúdez Cano and Ortiz Urbano, 1999; Bermúdez Cano et al. 2000; López Rodríguez, 2010, Jabalquinto et al., 2013, and Bascón., 2024) recognized tools and ceramic from Copper and Bronze Age, Tartessian and Iberian (VIII to I century BCE), Republican Roman (Ist century BCE), Imperial Roman (II century), Medieval (XIII-XV centuries) and Modern ages, that even today are easily recognized along the Castle Hill, with the Iberian period ceramic especially abundant. The castle was built by order of Fernández de Córdoba family along XIII and early XVI centuries,

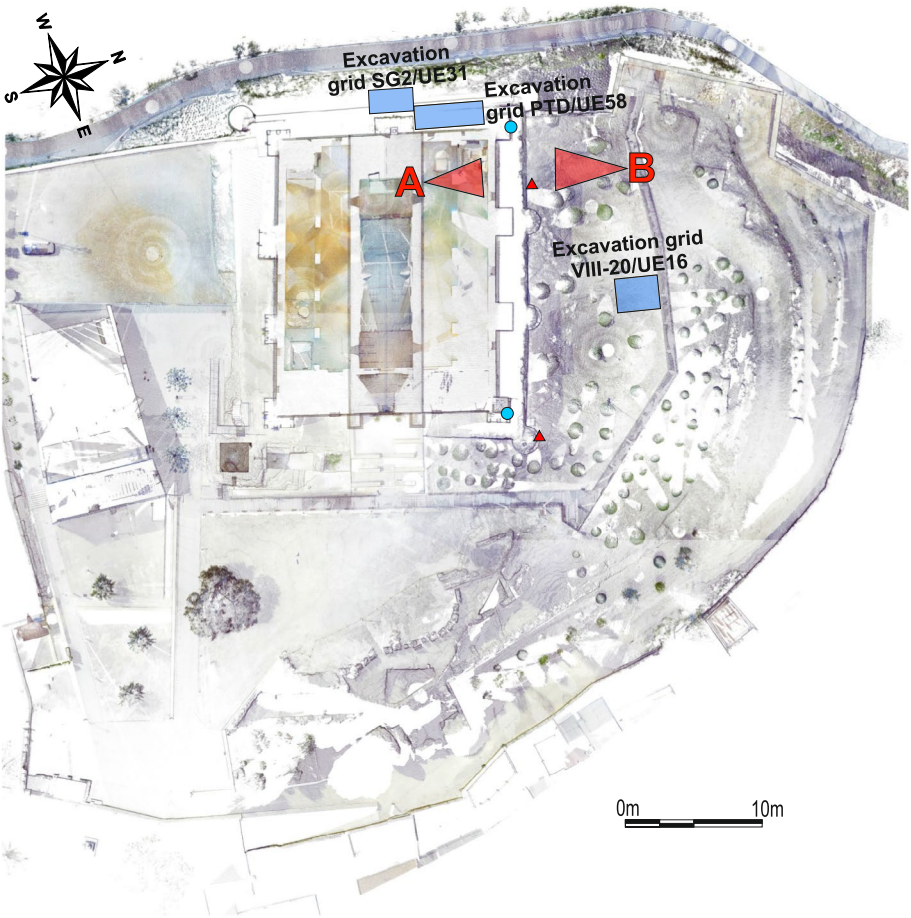

Fig. 2 Current Ducal granary at the top of Montilla Castle Hill laser image plan with location of the archaeological grids studied, wide angle of the camera for selected images (Point of view A corresponds to Fig. 20, left; point of view B corresponds to Figs. 19 and 21, right) and reference points along all images (blue dots and red triangles). Modified from Portero Delgado (2020)

located at the top of the slope. Different enlargements culminated in the construction of a large medieval fortress (Fig. 3) which, in 1508 AD, was partially demolished (just external curtain walls) by King Ferdinand "the Catholic" (reign from 1479–1516) as a punishment for the rebellious actions of Don Pedro Fernández de Córdoba, the first Marquis of Priego (Rey 2017). For unknown reasons, the fortress was abandoned and repurposed as a stone quarry during the XVI and XVII centuries, with only parts of the walls and foundations remaining today (Fig. 4).

In 1998 AD, the town government bought the Ducal granary. An extensive concrete foundation slab was constructed along the entire granary to prevent structural issues, and the NW facade was restored. To date, only admissible minor cracks in the covering walls have been observed in few places.

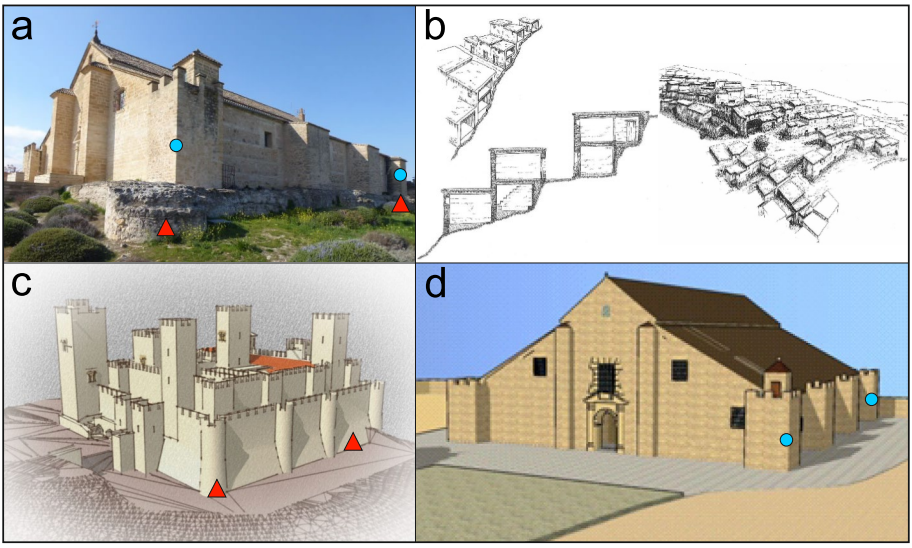

Fig. 3 Evolution of the structures recognized in the Montilla Castle Hill. **a** Current Ducal granary and basements of the Medieval Castle. **b** Typical Iberian-period town construction over hillslopes, following a terraced house structure (VII to Ist centuries BCE) example from El Tossal de Sant Miquel (Spain) (Bonet, 1995) **c** Approximate reconstruction of Montilla Castle (XV-XVI centuries) by Portero Delgado (2020). **d** Reconstruction of the XVIII century Ducal granary constructed over the castle ruins

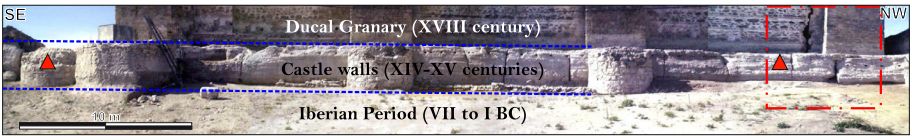

Fig. 4 Present day stratigraphy. Red triangles and blue dots are reference points to be compared with Figs. 2 and 3 among others. Red dashed square includes the landslide crown and associated cracks affecting old and recent structures (see Figs. 19 and 21 left for details)

The archaeological materials recovered from the Castle Hill sedimentary units are varied, ranging from construction materials (roof tiles, bricks, solid clay bricks), animal bone remains (cow, pig, sheep), charred seeds and plant remains, to ceramic fragments, which are very common at these deposits. Regarding the characteristics of the selected pottery, common or kitchen pottery predominates. The most common fragments belong to containers for storing food (jars and pots) and liquids (jugs, pitchers, flasks) with traditional shapes from the area. The archaeological contents of these levels are preserved in the facilities of the Archaeological Museum of Córdoba and the Local History Museum of Montilla. Much of this material is describe in the work by Ortiz et al. (2018), among other referenced reports.

2.2 Geological setting

The Montilla Castle Hill, which is the focus of this study, is located in the village of Montilla, in the southern part of the Iberian Peninsula (Fig. 1a, marked with a yellow star; Lat.

37.59233º N, Long. 4.63769º W). The hill has elevation difference of 74 m, ranging from 414 m a.s.l. (at the castle entrance) to 340 m a.s.l. (at the base of the NW hill flank) with an average slope of 5.5%. This study focuses on the north-western face which is the steepest and not urbanized. The sharp escarpment shape of this face is a consequence of the landslide activity.

Geologically, the hill consists of Triassic olistostrome formations at the bottom, and well-stratified Miocene materials at the top. The lithology are predominantly clays (~15 m thickness), marls (~20 m thickness), consolidate rock (calcarenites) at the top (0 to 6 m thickness), and anthropic deposits with variable thickness. The Triassic clays correspond to the so-called 'German-Andalusian' facies, an olistostromic formation that also containing gypsum and halite (Roldán García et al. 1985). The marls are stratified marine deposits from the Late Miocene, exhibiting an overall coarsening-shallowing upward trend overlain by calcarenites. The geomorphology of this region is controlled by differential erosion, with soft sediment (clay and marls) eroded away, leaving harder rocks (calcarenites) at the top of the hills (Roldán García et al. 1985).

2.3 Seismological setting

To explore the link between landslide reactivations and earthquakes in the Castle Hill, a detailed seismicity study was conducted. On July 5th, 1930, a damaging earthquake struck Montilla. Kárník (1969) catalogued the earthquake with a magnitude M_S 5.1, while the Spanish National Geographic Institute (IGN) cataloged it with a magnitude M_D 4.9 and a maximum felt intensity equal to VII. In a comprehensive study, Batlló et al. (2010) re-evaluated the coordinates and magnitude of this earthquake, as well as computed the focal solution through moment tensor inversion. The authors digitize and processed several records, most of them on smoked paper coming from mechanical seismographs. The obtained location, using a local model, is 37.556° N and 4.645° W, with an uncertainty of about 15 km in longitude and 12 km in latitude. It coincides with the previously supposed location from macroseismic data. The moment tensor inversion revealed a pure normal fault mechanism, as shown in Fig. 5, with a magnitude Mw 5.1. This solution, as highlighted by Batlló et al. (2010), is consistent with the regional stress pattern (e.g., Henares et al. 2003; De Vicente et al. 2008; Sparacino et al. 2020). Newspapers and a contemporary report (Carbonell 1930) clearly portrayed the felt effects. The shake duration was about 8 s being accompanied by seismic sounds. Significant damages occurred, but there were no victims. More than 250 houses were heavily damaged, and most of them suffered fissures. Additionally, there was also considerable damage to both civil (train station and hospital) and religious buildings. Recurrent damage, alongside fissures, included the sliding of roof sheathing and tiles, exposing the wooden rafters in many houses. The shaking also induced some water wells to overflow.

No other noteworthy historical earthquakes near the city have been documented. The most influential regional event was the 1755 Lisbon earthquake, which was felt with an intensity of VII, not only in this town but also in the surrounding areas (Martínez Solares, 2001). In Montilla, the shaking, which lasted for more than 7 min, led to significant damage to the bell tower of the church (Calvo Serrano et al., 2020), two monasteries and 52 houses. Although no geological effects related to the Lisbon earthquake are specifically mentioned, they cannot be ruled out, given the duration of the shaking and the documentation of such

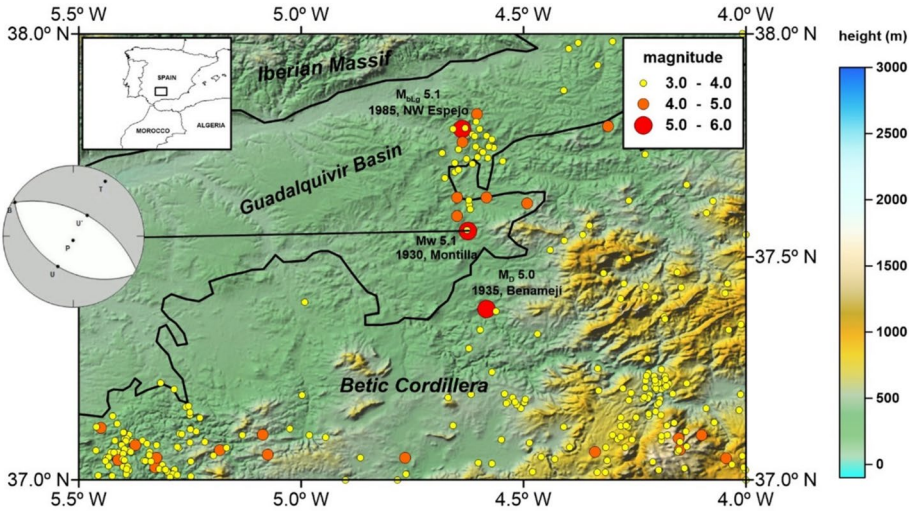

Fig. 5 Instrumental seismicity recorded up to 2020 in the surroundings of the Montilla Castle Hill. The most significant events are labelled. The computed focal mechanism solution for the 1930 earthquake is also included (Batlló et al. 2010)

effects in nearby locations. For instance, fissures in the ground were documented in the town of Luque (Córdoba) and rockslides in Montoro (Córdoba), both located within 60 km of the studied site, as well as landslide reactivations in Güevéjar (Granada), approximately 100 km away (Sanz 1997; Lenti et al. 2016).

3 Methods

3.1 DC electrical surveys

Resistivity determines the difficulty of the electric current flow through a material independently of its shape. Electrical resistivity tomography allows for determining the underlying electrical resistivity structure by the injection of an electric current via a pair of steel electrodes and measuring the potential difference using a second pair of electrodes. Varying electrode configurations enable the calculation of apparent resistivity at different depths, accounting also for lateral variations. This method involves calculating ground resistivity from apparent resistivity through data inversion, which can then be interpreted in geological terms.

In the case of polarizable grown, upon interrupting the current, the voltage rapidly decreases until it reaches a value beyond which the slow exponential decay occurs. This behavior is called Induced Polarization (IP) and allows inferring the presence of bodies with metallic conductivity (such as certain metallic minerals and graphite) or clays (Everett 2013; Martinez-Moreno et al., 2018).

Two parallel transects (approximately 140 m long in the horizontal real distance) were measured using the ABEM Terrameter SAS 4000 device with resolution of ± 1 μV and an electrode spacing of 2 m. The instrument injects current to measure the resistivity of the

subsurface, latterly stopping injection monitoring the IP, with the transient voltage decay in several time intervals. The profiles were acquired with a multichannel multiple gradient electrode array. The gradient protocol used the Wenner-Schlumberger configuration adapted to multichannel resistivity meter systems.

Data inversions were calculated by means of RES2DINV software (v.3.59; AGS Aahrus Geosoftware Inc.) using the standard least-square method and model refinement constraint due to the larger amount of data (Loke, 2019). Other parameters used were a mesh made up of model cells, 4 nodes per unit electrode spacing, an initial factor of 0.3, reducing the effect of the side blocks and finite elements with trapezoidal elements.

The normalized depth of investigation (DOI) index, indicating the extent to which the model is constrained by the data, was calculated for all profiles. This calculation is based on the inversion of the profile with two different resistivity values for the initial models. Later, the value on each cell is compared in both inversion and calculated the normalized one. The main difficulty is deciding the cut-off value where the inversion is reliable. Marescot et al. (2003) recommended a cut-off value of 0.1–0.2, although in this work it was used the more restrictive value of 0.1.

3.2 Geotechnical modelling

Slope stability was analyzed using profiles defined by limit equilibrium methods based on the slice technique. Among these, the Bishop, Morgenstem-Prize, Jambu, and Spencer methods were applied (Bishop 1955; Janbu et al. 1956; Morgenstein and Price 1965; Spencer 1967) using the Rock Science Slide software. A geotechnical model has been developed, and a steady-state model was calculated to assess the effect of rain. For the seismic input, values above 0.06 g, the basic seismic acceleration defined for Montilla in the Spanish resistant regulations (NCSE-02, 2002), were considered.

At the same time, the calculated deformation was studied to estimate the deformation rate that may occur on the slope, considering the potential effect of rainfall and seismicity. For this purpose, the Rockscience Phase2 software was used.

Regarding the effect of rainfall, it was assumed that both the central and lateral parts of the slope have the same permeability. While this represents an unrealistic scenario, it is considered to be highly conservative.

The study has been carried out on two representative calculation profiles, taking into account the stratigraphy of the terrain, as well as the tectonic and hydrogeological conditions. These profiles were defined based on the detailed geological and geophysical investigations carried out in this work and its surrounding environment, along with data from the LABSON report.

Based on the geological profile at the site, three units were defined for the analysis profiles. The parameters used in the calculations are summarized in Table 1.

Table 1 Geotechnical parameters for extended profiles P1 and P2

Profile	Security Factor (SF)	NCSE-02 Limit SF	Maximum sink estimated for Ducal granary (cm)	Admissibility (edification code) limit for Ducal granary (cm)	Maximum sink estimated for Córdoba road (cm)
1	1.3	1.2	8.8	15.0	0.8
2	1.76	1.2	14.0	15.0	2.0

In this study, to account for additional natural phenomena that, together with seismicity, could trigger a landslide and reduce the safety factor to values below 1, a uniform surface infiltration rate was incorporated into the model along the entire slope. This rate represents the peak precipitation recorded over the past 10 years expressed in liters per hour (l/h). The value used was 20.16 l/h, corresponding to a daily precipitation of 483.8 l/d. As a result, the slip probability (SF < 1) increases to values exceeding 70%.

3.3 Seismic modelling

Based on the previous geotechnical model, the stability of the slope in variable seismic conditions of the study area was estimated.

To carry out the calculations for this investigation, it was used PHASE2 v. 8.2 software to make a FEM model of the slope, from the construction under study to the road, using stablished geotechnical parameters. A calculation routine was executed for different seismic coefficient values, ranging from values lower than the defined value for the study area (0.06 g), to higher values (0.25 g), in order to consider the obtained design spectrum developed to account the 1930 Montilla event. In all cases, the critical safety factor (FCR) was calculated. The point at which FCR is = 1 was identified in the resulting point cloud, as this value represents the strict equilibrium.

The safety factor was calculated using the RockScience software PHASE2 v.8.2, which employs finite elements. To determine the stability of slopes, a formulation called "Critical SRF" (Critical; Stress Reduction Factor/ Reduction of Shear Resistance) is used. This method involves progressively reducing the resistance parameters by a certain percentage and verifying the new stability of the system. If the system remains stable, the resistance parameters are further reduced until the system becomes unstable. In this manner, the critical resistance factor, or safety factor, for the study area is determined.

3.4 Absolute and relative chronology

The absolute ages of various events are based on two radiocarbon dates obtained using Accelerator Mass Spectrometry (AMS) on organic materials (Table 2). These measurements were conducted at the Isotope Research and Poznan Radiocarbon Laboratory (Poznan, Poland). In order to compare data with historical events all ^{14}C-AMS ages were calibrated to calendar years (cal. BP) with OxCal 4.4 (Ramsey, 2009) based on the IntCal20 Northern Hemisphere radiocarbon calibration curve (Reimer et al. 2020).

The archaeological relative chronology was established through the analysis and classification of ceramic materials found within each stratigraphic units–whether they are earthen

Table 2 Results of AMS ^{14}C dating of charcoal material from different archaeological levels from the Montilla Castle Hill

Sample	Lab. code	Conventional age	Calib. age	Probability	Material
Mont-PTD UE58 BOL22	Poz-53607	2295 ± 35 BP	408–208 cal BCE	95.4%	Charcoal
Mont-VIII 20 BOL90 UE16	Poz-53608	490 ± 30 BP	1404–1452 cal CE	95.4%	Charcoal

(strata) or built (structures)–excavated during five archaeological campaigns at the studied site.

To assign the ceramic pieces to specific chronological periods, a comparative approach was employed using various established typological studies. The used typologies include:

- Handmade ceramic or '*tosca*': smoothed and burnished (Ruiz Mata (1995), Murillo (1994)); incised decoration (Ruiz Mata (1995), Ladrón de Guevara 1994); 'Almagra' (red ochre) pottery (Buero (1988).
- Ceramics on potter's wheel: Amphorae (Pellicer (1978); Florido (1984), Guerrero (1991), Ramon (1995)); Common and wheel-painted pottery (Escacena (1987), Pereira (1988a, 1988b, 1989), García Vargas et al. (1989), Vaquerizo et al. (1992)).
- Other ceramic types: Gray ceramics (Roos (1982), Caro (1989), Murillo (1994)); red slip ceramic (Negueruela (1980), Rufete (1989)).

4 Results

The northwestern face of the Montilla Castle Hill is affected by a set of laterally interconnected rotational landslides (Fig. 6). The uppermost part of these landslides is determined by a well-defined general crown (approximately 500 m in length) related to the presence of a hard calcarenite layer forming the hilltop (Fig. 6). Several crown cracks have caused structural damage to the building. The main scarp, which follows the crown, extend for 90 m, and present an elevation difference of 28 m, with a maximum slope of 16.3º. This area marks the steepest section of the slope and has developed in marls beneath the calcarenites. The base of the scarp curves upward, giving rise to a concave topography characteristic of the erosion zone. In contrast, the accumulation zone distinguishes an upward convex shape, terminating at the landslide toe, located approximately 250–300 m downslope from the crown.

4.1 Landslide structure from ERT and IP

The location of the ERT and IP profiles in relation to the landslide boundaries is indicated in Figs. 6 and 7. The resistivity sections (Fig. 8a and c), show resistivity values ranging from 1 to approximately 250 Ω·m for profile P1, and from 1 to around 500 Ω·m for profile P2. Profile P1 reveals two main domains with distinct electrical characteristics. The upper layer is resistive, corresponding to detached sands and calcarenites fragments, together with archaeological remains. In contrast, the lower layer is conductive due to the presence of marls (green scale colours) and Triassic clays (blue scale colours). Profile P2 exhibits similar features although the conductive layer appears more widespread. The boundaries between resistive and conductive domains exhibit a rough vertical to convex shape in the upper levels, and subangular to horizontal configuration in the lower sections. The IP models (Fig. 7b and d) show moderate chargeability values of approximately 4–6 ms throughout the profile P1. In profile P2, chargeability values range from mostly ~ 1 ms to ~ 30 ms in the deepest northwest part. These high chargeability areas are indicative of clay-rich layers.

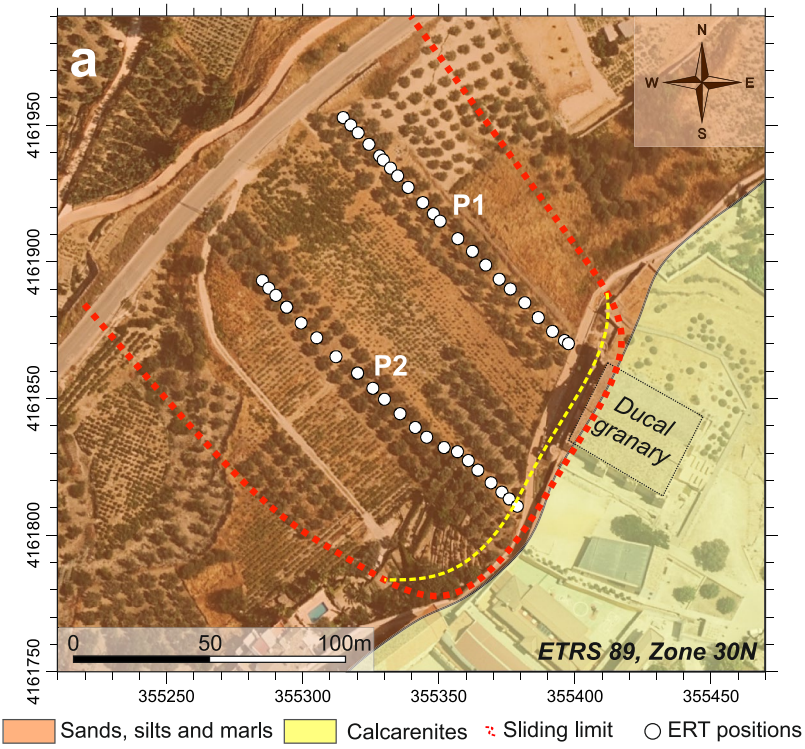

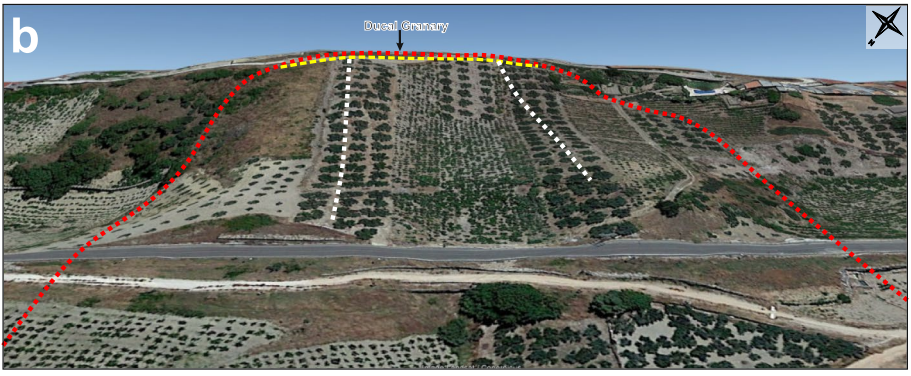

Fig. 6 Location of the study area showed in Fig. 1. **a** Castle Hill of Montilla and location of the two ERT profiles (P1 and P2). White points represent electrodes position. Dashed line depicts the present-day lithological contact between calcarenite rocks and soft anthropogenic/marls sediments. Ducal granary limits can be observed with the north-west facade emplaced over the marls. **b** Frontal view of the studied landslide (3D image from Google Earth). Red dashed line depicts landslide boundaries. Yellow dashed line represents ancient landslide crown

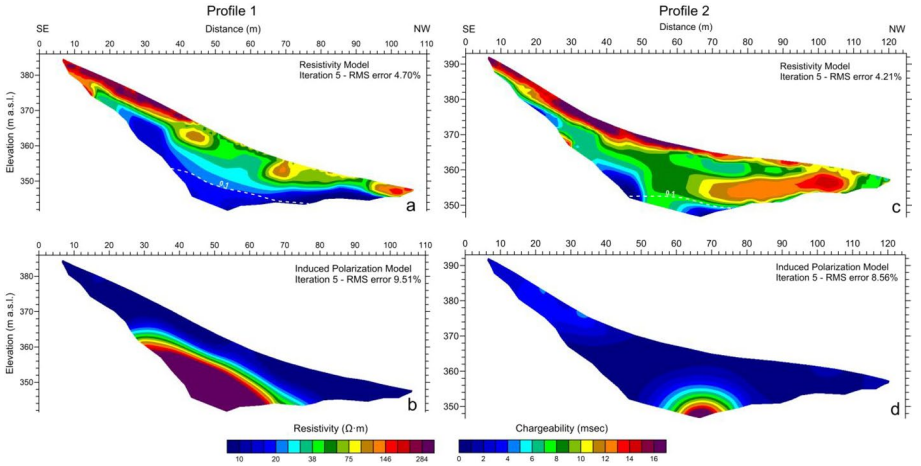

Fig. 7 Inversion models of ERT (up) and IP (down) profiles along the landslide. The 0.1 DOI index value is marked with white dashes lines. **a** Resistivity model, and **b** IP model for profile P1. **c** Resistivity model, and **d** IP model for profile P2

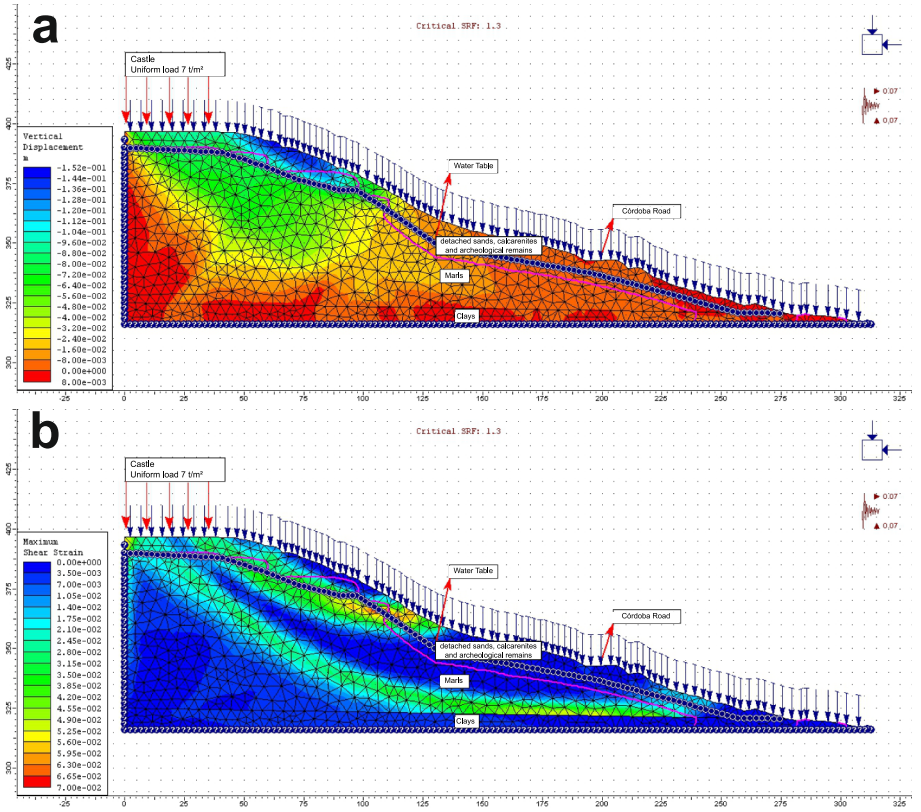

Fig. 8 Geotechnical features of the Montilla Castle Hill landslide. **a** Vertical displacements along profile P1. **b** Critical circles, deformations and maximum shear along profile P1

4.2 Geotechnical analysis and modelling

Using the aforementioned methodologies, analysis of slope stability, seepages and deformation analyses have been conducted obtaining the following results. Figures 8 and 9 shows the distribution of vertical displacements along profile 1 (Fig. 6a), including displacement vectors relative to both the initial state and the current condition. These figures also incorporate projected displacement resulting from the loading of the Ducal granary, the layout of the Córdoba road (Fig. 8), the seismic conditions and the project-specific rainfall impact. The maximum movements expected along this profile are anticipated to occur in three areas: the loading zone at the crest, the area beneath the road, and the foot of the slope. The most significant movements are anticipated near the Ducal granary, situated at the top of the slope, where multiple factors converge: hydraulic loading, weigh of the structure itself and the progressive steepening of the hillside. Additionally, material extraction at the foot of the slope during the road construction likely triggered initial destabilization, which resulted in a series of slope movements.

The final position of the water table is observed, which clearly defines the zones of hydrodynamic tension and decompression with a good correlation between all of them.

The critical stability results are expressed in terms of Safety Reduction Factor (SFR) in Fig. 8. The zones of the critical slip circles can also be observed. Two slip circles are identified along the direction of maximum slope. The first is located at the foot of the slope, contributing to the depressions observed in the middle of the slope, while the second is deeper, originating outside the slope and extending into the plastic clay basement.

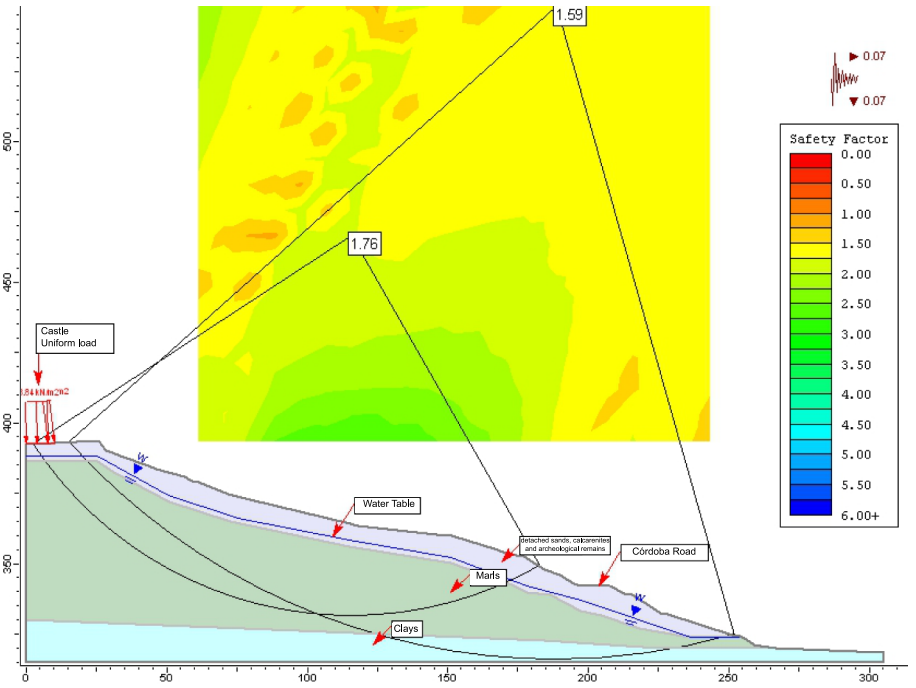

Fig. 9 Castle Hill security factors and potential circular slip surface along Profile P2

The limit equilibrium results for the worst slip circle suggest that stability conditions are satisfied in nearly all the scenarios analysed, according to the imposed requirements (see Sect. 4.3). The factor of safety consistently exceed 1.2, which is the threshold for seismic conditions as outlined in the current slope stability.

4.3 Seismicity and seismic modelling

Since no ground motion data have been recorded at this place, a design spectrum has been developed for Montilla using the PEER (Pacific Earthquake Engineering Research Center) ground motion database, i.e., the NGA-West2 database (Next Generation Attenuation). To do this, specific records were searched based on predefined criteria. In this case, the search criteria included earthquakes with a similar magnitude and faulting type to the 1930 Montilla earthquake, and records from similar distances and site conditions (Fig. 5). The objective is to predict the ground motion for an earthquake with the same characteristics and in the same location as the 1930 earthquake.

In an initial search, the following criteria were applied: (i) a magnitude range equal to Mw 5.0–5.2, (ii) normal fault mechanism, (iii) a distance to the rupture less than 10 km, and (iv) V_{S30} in the range 400–600 m/s. Only one record was found. In a subsequent search, the magnitude range was extended to Mw 4.9–5.3. Obtained records in this new search correspond to the 1977, Mw 5.3, Izmir (Turkey) earthquake and different aftershocks of the 1997–1998 Umbria Marche (Italy) sequence. The significant duration (5–95% of Arias Intensity) ranges from 1.6–4.5 s. The average (design) spectrum (5% damping ratio) including mean ± standard deviation curves are displayed in Fig. 10, as along with the spectrum of the record obtained in the more restricted search, which corresponds to an aftershock of the 1997–1998 Umbria Marche sequence with magnitude of Mw 5.1.

The obtained pseudo-spectral values (Fig. 10) for very low oscillation periods (0.01 s), i.e., peak ground acceleration values, range from 0.22 and 0.50 g, with a mean value of 0.33 g. For instance, mean values of 0.62, 0.63 and 0.87 g have been obtained for oscillation periods of 0.05, 0.1 and 0.15 s, respectively. These results must be considered as a design or target response spectrum or a deterministic scenario earthquake spectrum, not as a uniform hazard spectrum. This information has been combined with the geotechnical model to predict Castle Hill sensibility to varying seismic conditions (above mentioned in Sect. 3.3). According to conducted simulations (Fig. 11), ground accelerations of the order of 0.17 g imply a critical stability coefficient equal to 1.0. From the design spectrum (Fig. 10), this is a ground motion value which was most likely exceeded during the 1930 earthquake, a Mw 5.1 event near the location. Obtained values also point that the Montilla Castle Hill slopes could be sensitive to major earthquakes located in SW Iberian margin, which can reach maximum felt intensities of X along the Atlantic coast, and VII where Montilla is located (Fig. 12).

4.4 Absolute and relative ages

Two samples of charred material were submitted for radiocarbon analysis to the Poznan Radiocarbon Laboratory (Poland) in 2013 following an archaeological campaign. The first sample consisted on two small charcoal fragments from an ash layer (Mont-VIII 20), and the second was a fragment of charcoal wood (Mont-PTD UE58; Fig. 13 and Table 2). The calibrated date for sample Mont-PTD UE58 falls into two separate intervals, due to the shape

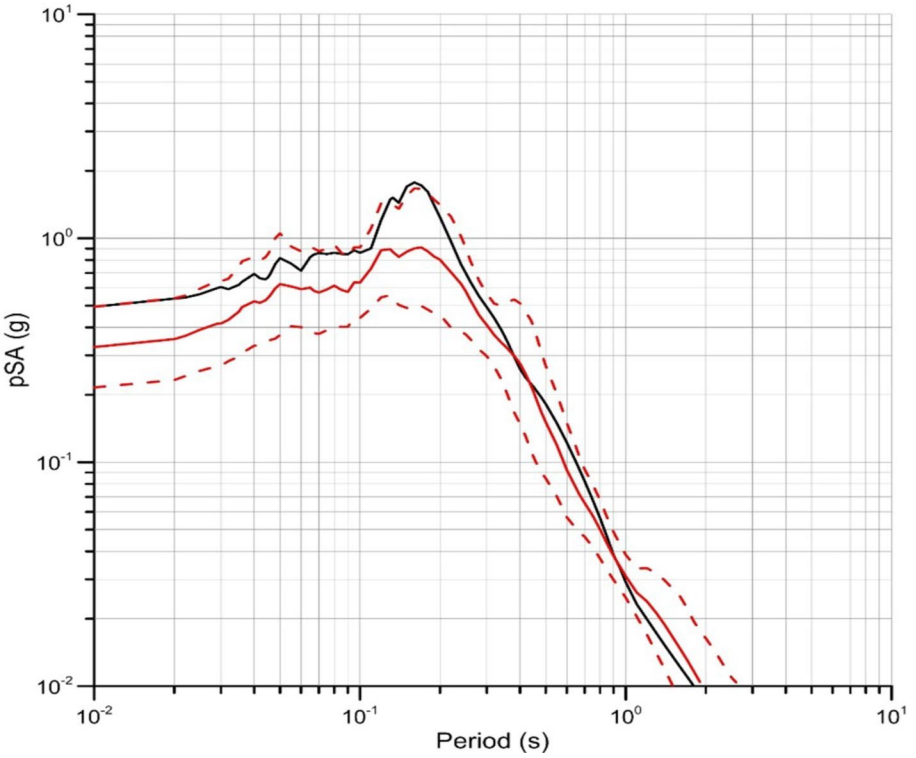

Fig. 10 Design spectrum for the Montilla Castle Hill. The mean value is represented by the red solid line, while the red dashed lines indicate the mean± The black solid line corresponds to an aftershock of the 1997–1998 Umbria Marche sequence (see text)

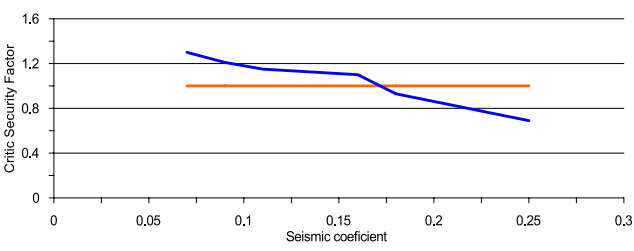

Basic seismic coeficient of acceleration (ab/g)	Critical Stability Coefficient (Critical SRF)
0.07	1.3
0.09	1.21
0.11	1.15
0.16	1.10
0.18	0.93
0.25	0.69

Fig. 11 Montilla Castle Hill slope seismic threshold. Blue line corresponds to Castle Hill critical SRF vs (ab/g) and orange line correspond to critical stability coefficient

of the ^{14}C calibration curve during this period. The older interval, between 408 to 351 yr cal BC (~380 yr BC) has a higher probability (58.8%), being supported by archaeological evidence, particularly ceramic remains. The younger interval, between 296–208 yr cal BC, while less probable (36.6%), cannot be entirely ruled out. The second sample, Mont-VIII 20, yield a calibrated date of 1404–1452 AD (95.4%) (~1448 AD; 490±30 yr BP ^{14}C). This date aligns closely with historical records indicating major reconstruction work at the

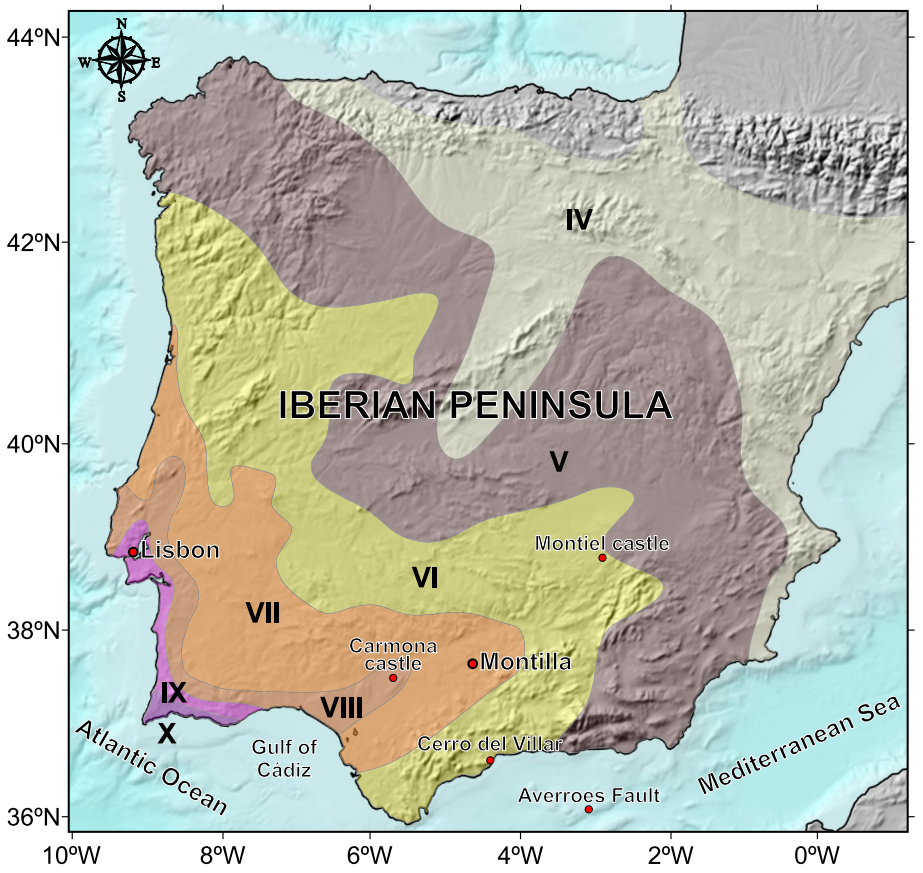

Fig. 12 Intensities of the 1755 Lisbon Earthquake felt in the Iberian Peninsula (Modified from Oliveira, 2008). The location of the Montilla Castle Hill is indicated and other sites included in the discussion

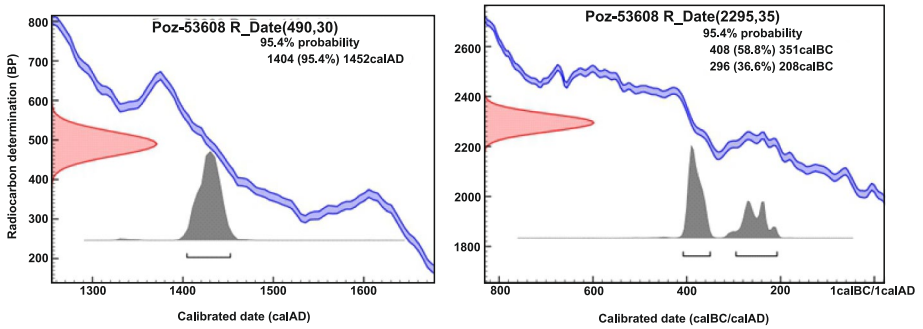

Fig. 13 Radiocarbon determinations from the studied archaeological sections in the Montilla Castle Hill. The conventional and calibrated age probability with 2 standard deviation from castle foundations (right), and ash layer associated to landslides (left)

site during this period, making its establishment as the main residence of the Fernández de Córdoba family (Rey 2017).

Ceramic and other archaeological remains indicate levels of Copper and Bronze Age, Iberian (VIII to I century BCE), Republican Roman (first century BCE), Medieval (XIII-XV centuries) and Modern ages (e.g., Bermúdez Cano and Ortiz, 2001).

5 Discussion

5.1 Castle hill landslides, structures and triggering factors

ERT research carried out on the Montilla Castle Hill has helped to constrain not only geological features but also the internal structure of the landslide, as well as the presence of possible archaeological remains (Fig. 14). According to surface observations, anthropogenic elements correspond to electrical resistivity values higher than 125 Ω·m (represented in dark red to purple colours in Fig. 14b), while geological materials display lower values:

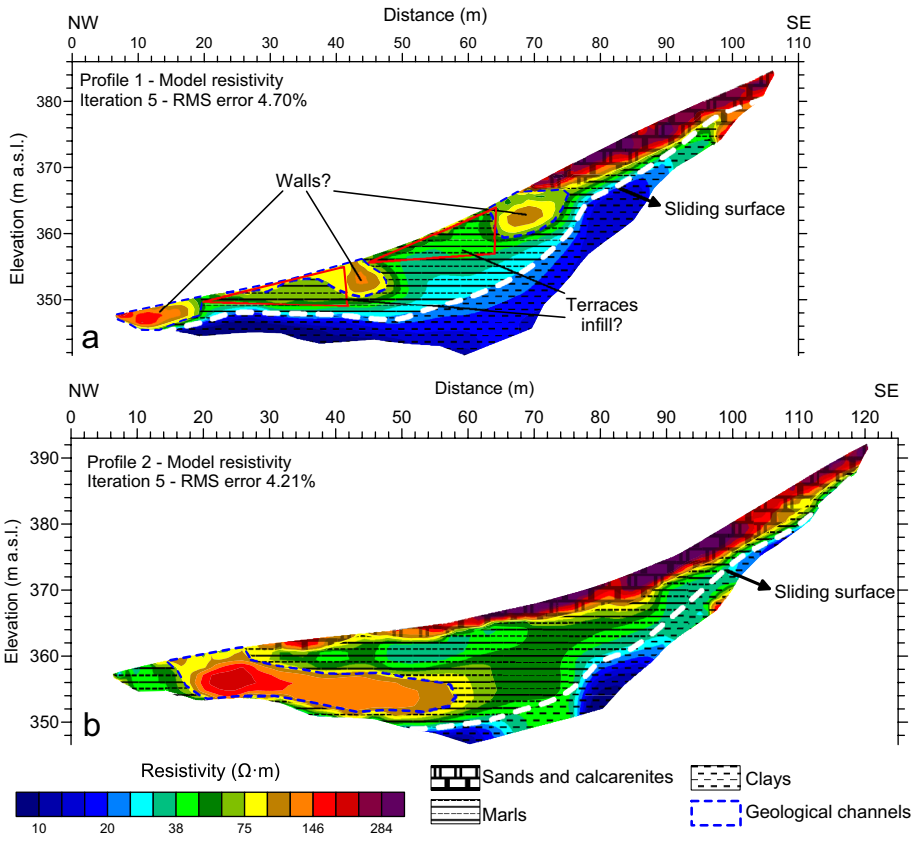

Fig. 14 Interpretation of the ERT profiles highlighting the main new observed features in **a** profile P1, with likely walls and terraces infill, and **b** profile P2. Most resistive materials at the top are a mix of detached sands, calcarenites and archaeological remains

clays and marls range from 1 to approximately 50–60 Ω·m (blue to light blue-green in Fig. 14b), and silts, sands and calcarenites range from 60–125 Ω·m (yellow to red).

Fracture zones were particularly well identified by the ERT data, enabling to describe landslide, their internal structure, and the potential location of future rupture surfaces. The fractures detected through ERT align well with those predicted by the geotechnical modelling (Fig. 8). Zones of lower resistivity appear to be associated with convex geometries, such as those typically associated with landslide rupture surfaces.

In profile 1 (Fig. 14, top) a transect reveals a curved surface characterized by low resistivity, which is consistent with a landslide rupture surface enriched with saltwater. The presence of saltwater likely contributes to reduce the resistivity compared with the surrounded materials (Telford et al. 1990; Reynolds 2011). The described characteristics align with a rotational landslide, following the classification proposed by Varnes (Hungr et al. 2014), likely involving progressive reactivations along a major rupture surface. This ERT profile does not cross the toe of the landslide, which is located in a lower topographic level, nor does it capture the most recent landslide crown and scarp affecting both the excavated archaeological layers and Ducal granary (Fig. 15). The presence of a road, walls and other building structures prevented the extension of the ERT profile to include these additional elements.

Along the hillside slope, at least three high resistivity rectangular bodies can be identified at shallow depth (Figs. 14 and 15). These bodies are interpreted as anthropogenic structures, most likely representing walls between 2 and 5 m in heigh. The tops of these walls are associated with flattened surfaces displaying resistivity values of approximately 75 Ω·m (Fig. 14a), which appear to have been filled with high-resistivity anthropogenic sediments (e.g., ceramics, construction debris, etc.) in a wedged-like configuration. One of these structures was partially excavated at the top of the Castle Hill, and described as thick walls composed by calcarenite rock blocks (Jabalquinto et al. 2020). This suggest that sections of the hillside were levelled in the past. Terracing and retaining walls were commonly constructed by Iberian communities during the Iron Age (VII to II centuries BCE) on hilltops, as documented at various archaeological sites such as Cerro de Santa Cruz (Almedinilla, Córdoba) (Abelleira et al. 2020) and El Tossal de Sant Miquel (Bonet Rosado 1995), among others (Fig. 3b). However, based on current data, we cannot determine the exact period in which these terraces were constructed or their intended purpose (whether to improve slope stability, expand agricultural land, serve defensive functions, or otherwise). Notably, at least one of the retaining walls or ramparts, located at ~360 m a.s.l., appears to be associated with a landslide scarp, indicating that this terrace may have been constructed after this landslide occurred (Fig. 14a, distance 75 m). If the terrace had been constructed prior to the landslides, the presence of back-tilted components indicative of rotational movements would be expected; nonetheless, these are not present in the current terrace structures.

Profile 2 displays many similarities with profile 1. The major rupture surface associated with the landslide can be identified at approximately the same elevation (~350 m a.s.l.), as along with a corresponding head and scarp at same level (Fig. 14b). The main difference with profile 1 lies in the presence of two extremely low resistivity bodies (blue colours in Fig. 8a and c), which are interpreted as saline water masses. Saline and evaporite deposits are common throughout the entire Guadalquivir Basin, and are associated with the Triassic olistostromic complex, which contains gypsum and halite (Calaforra and Pulido-Bosch 1999; Perez-Valera et al., 2017). The presence of underground saline water beneath the

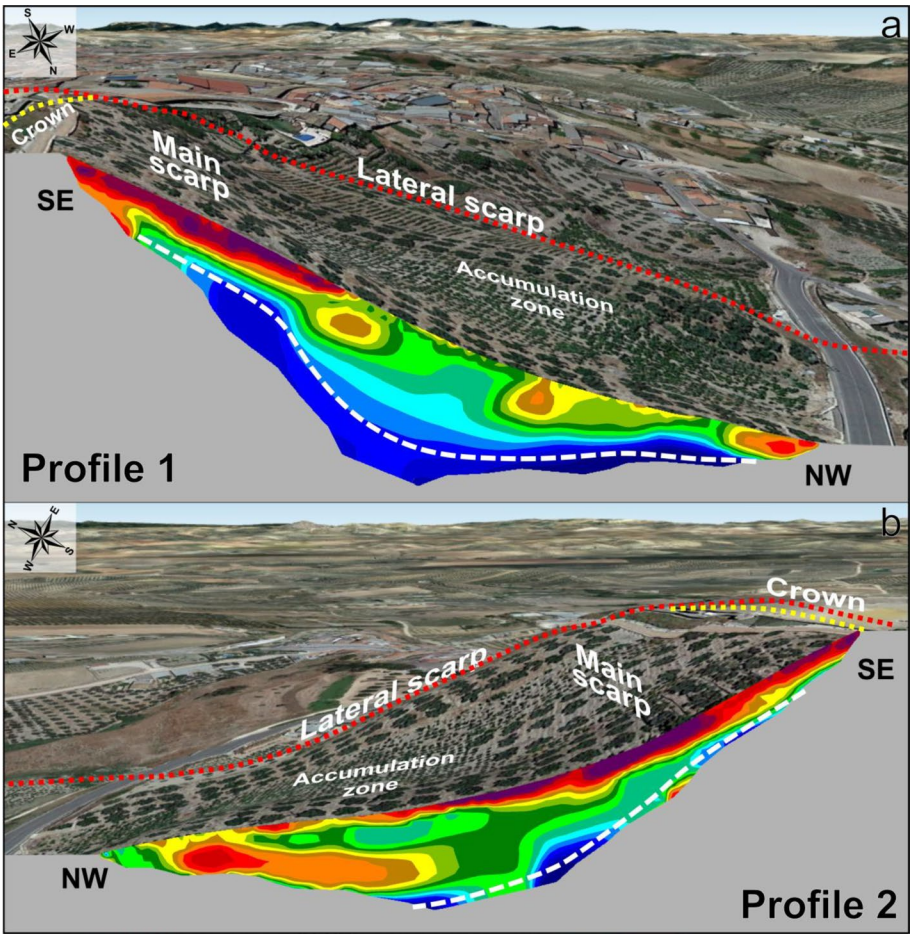

Fig. 15 Landslide surface and ERT models (3D images from Google Earth). **a** Cross section along profile P1. **b** Cross section along profile P2. Yellow dashed line represents ancient landslide crown affecting Iberian period archaeological levels

Montilla Castle Hill is further supported by historical records referring to the well-known "Poza de la Lagaña", whose saline waters were once used for medical purposes. Brown to orange colours observed at the base of the sequence (Fig. 15b) may be attributed to channel facies, which are typical within the Tortonian-Messinian facies (Aguirre et al. 2022). In this profile, evidence of terracing is less apparent.

The features of the landslide surface are clearly discernible in the ERT profiles, as depicted in Figs. 14 and 15. The main scarp, characterized by abrupt topographic changes and the juxtaposition of calcarenites above Triassic material, is identified as a zone of high resistivity, contrasting with lower resistivity values observed at depth. Furthermore, the accumulation zone, where the topography becomes more levelled, is distinguished by medium to low resistivity values.

Based on ERT models and field observations, it can be inferred that a key factor associated with the studied landslide is the presence of a slope mostly composed of Miocene

marls, silts and calcarenites overlying Triassic materials, primarily consisting of lutites and evaporites. The main rupture surface is located at the top of the low resistivity and high chargeability lutite layer, corresponding to the contact between Triassic olistostrome and the Miocene marls (Fig. 7). Similar geological and geotechnical conditions have been documented in other landslide-prone areas within the Guadalquivir Basin and various complexes of the Betic Cordillera (e.g., Fernández et al. 2021).

The marls at Castle Hill are equivalent to the so-called 'blue/white marls', which have been geotechnically characterized in previous studies as high plastic, medium–high expansion and low strength parameters (Escolano et al. 2019). These Miocene marls behave similarly to stiff soil, often classified as over-consolidated clays, and are characterized by fragile shear strength and degradation after drying and wetting processes, which can lead to sudden geotechnical failure (Vazquez-Boza et al., 2014).

The most important factor triggering instability in such marls is intense rainfall, which significantly increases pore-water pressure (Escolano and Bueno 2015). Additionally, the presence of highly porous calcarenites forming a confined aquifer above the marls in the studied location further contributes to affect pore-water pressure. Nonetheless, these materials are subject to sudden instability, generally attributable to excavation processes. In south Iberia, moderate to strong earthquakes have been identified as triggers for landslides (Delgado et al. 2011a; Alfaro et al., 2021), even low to moderate events (Delgado et al. 2011b). Therefore, the possibility that seismic activity could affect the studied slope cannot be ruled out. Although the slope is currently stable, seismic modelling suggests that it could be reactivated by local low to moderate earthquakes.

5.2 Iberian period: synchronous landslides and destruction levels

During five archaeological campaigns at the Castle Hill, two distinct destruction events have been identified, both associated with ash layers, collapsed walls, and titled anthropic floors, likely associated with slope instability processes (Bermúdez Cano et al. 2000) (Figs. 16 and 17). The first evidence of archaeological levels affected by landsliding (referred to as Montilla landslide-1, MS-1 in Fig. 16) corresponds to levels dated between 650 to 550 BCE (7th to sixth centuries BC), excavated in area SG2/UE31 (Fig. 2), based on diagnostic ceramic typologies (Bermúdez Cano et al 2000). The second event (MS-2), slightly more recent

Fig. 16 Stratigraphic profile of Iberian period archaeological levels, dated between 650 to 550 BCE (7th to sixth centuries BC), and excavated in area SG2/UE31 (Fig. 2): **a** original photography and **b** interpreted image. A wedge-shaped ash layer is observed, covered by horizontal bedded building debris

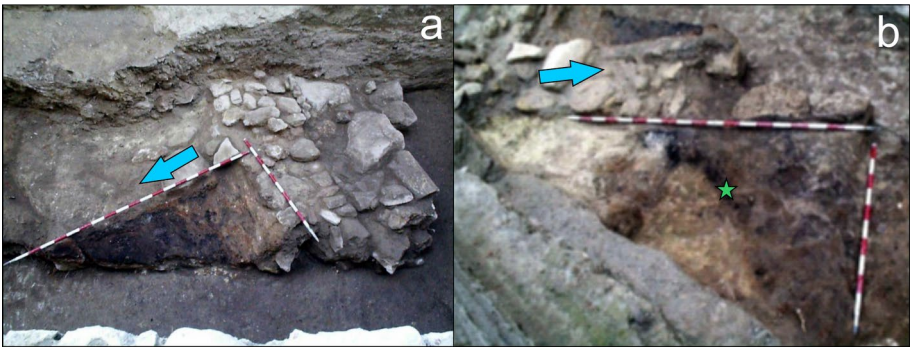

Fig. 17 Two views of the plan of Iberian period archaeological levels dated between 400–300 BCE (fifth-fourth centuries BC), and excavated in area PTD/UE58 (Fig. 2), based on characteristic ceramic types (Bermúdez et al., 2000) and a radiocarbon date (408–351 BC (58.8%) or 296–208 BC (32.6%)). The green star indicates the location of the radiocarbon sample, and the blue arrow points the wall debris with the same orientation, which covers the wedge-shaped ash layer

(~400–300 BCE, fifth-fourth centuries BC) (Fig. 17) excavated in area PTD/UE58 (Fig. 2), and dated though both characteristic ceramic and a radiocarbon date (Table 2, Fig. 13).

In both cases, stratigraphic evidence shows trampled levels or pavements dipping approximately 9º NW, covered by a wedge-shape sedimentary deposits rich in debris, ash and charcoals (Fig. 16b). Notably, the base of ash wedge follows the dipping orientation of the tilted pavement, while its upper layer is horizontal and sealed by collapsed wall remains (Fig. 16b). This sedimentary structure is interpreted as the result of a sudden hillslope collapse, which caused tilting of the occupation surfaces, followed by a rapid succession of fire and structural collapse (roof and wall). Such a pattern of destruction (comprising ground shaking, slide, fire and structural collapse) is frequently observed in urban settings affected by major earthquakes (Sekizawa 2023; Scawthorn et al. 2023). Alternatively, the possibility of an intentional burning or demolition of buildings following slope instability cannot be ruled out, particularly if the structural integrity of constructions had already been compromised by the landslide.

To discern whether these events were local or regional, and thus potentially associated to major earthquakes, the obtained dates were compared with historical, seismic and paleotsunami records from the Iberian Peninsula (Gràcia et al. 2010; Lario et al. 2011) (Fig. 18). Historical sources indicate various earthquakes occurring at 500, 348, 241, 216, 211, and 210 yr BC (Ocampo 1553), though recent reviews have questioned their reliability (Álvarez-Martí-Aguilar 2020). The paleotsunami record from the southern Iberian Peninsula identifies two tsunamigenic areas associated with major earthquakes: one in the Atlantic (Gulf of Cádiz/Gorringe ridge) and the other in the Alboran Sea (Fig. 1) (Vázquez et al. 2022). A catastrophic high-energy marine event has been documented in the area of Málaga, specifically at the Phoenician settlement of Cerro del Villar (Málaga), dating to the late seventh century BCE (625–600 BCE), which has been associated with a tsunami (Álvarez-Martí-Aguilar et al., 2022b). If the layer from Cerro del Villar, located at 120 km south of the studied site, is contemporaneous with the oldest destruction layer identified at the Montilla Castle Hill, it could represent the first evidence of major earthquakes, with magnitude of~7.0 placed in the Alboran Sea, as predicted by various studies (Estrada et al. 2021; Outiskt et al. 2025). Nevertheless, it cannot be ruled out that the introduction of new agricultural technologies

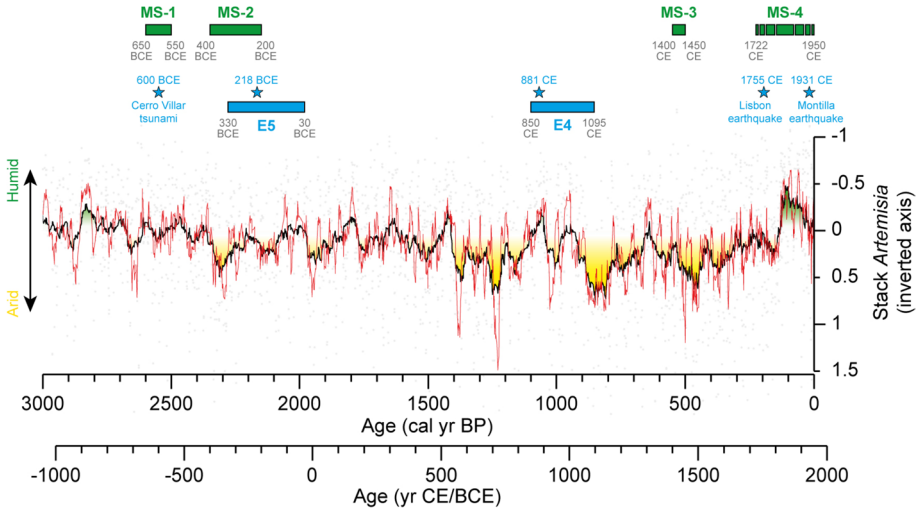

Fig. 18 Historical, seismic and paleotsunami catalogs of the Iberian Peninsula compared with phases of slope failure recognized at the Montilla Castle Hill (MS-1, MS-2, and MS-3 and MS-4). The stars indicate evidence of tsunamis or moderate earthquakes in southern Iberia. The stacks of the arid-adapted *Artemisia* and xerophytes taxa represent a compilation of climatic trends for the Iberian Peninsula (Camuera et al. 2023)

and the intensification of farming during the Phoenician colonization may have influenced hillside stability, contributing to landslides and major flooding affecting early settlements in Málaga, particularly in the Guadalhorce Delta at Cerro del Villar.

The evidence of a tsunamigenic event at the Gulf of Cádiz, coetaneous with the second landslide described at the studied site, is clearer. This event, referred to as Event 5 (Gràcia et al. 2010) (Fig. 18), has been dated at 330–30 BCE (2,280–1,980 yr cal. BP) based on turbiditic layers. However, in shallow and coastal sediments, the event appears to be dated ~ 218 BCE (Rodríguez Vidal et al., 2011; Ruiz et al. 2013), suggesting a magnitude of Mw 8.0. A Carthaginian shipwreck at the entrance of the Melilla harbour (Alboran Sea), has been also dated to between ~ 220–210 BCE based on recovered coins (Gozalbes 1991), which may also be linked to the tsunami event or to the ongoing conflict of the Second Punic War (218–201 BCE). At the studied site, the radiocarbon date from the wedge-shaped ash layer indicates an age ranging from 408 to 208 BC (Table 2), with the older interval (408–351 BCE) being more probable (58.8%) than the younger one (296–208 BCE, with a probability of 32.6%), all in agreement with recovered ceramics. This lack of precision is related with uncertainties in the radiocarbon dating process, but in any case, the date falls within the timeframe supported by marine, coastal and archaeological evidences pointing to a tsunamigenic event during this period.

Both episodes of slope instability must have had an impact on the daily life of the settlement. Despite the movements that affected part of the constructions (Figs. 16 and 17), the inhabitants continued to settle on the hilltop. They addressed this instability by demolishing the affected buildings, infilling and levelling the land, and using debris from previous wall as foundations for new constructions (Fig. 16). Likely, after one of these slope movements, they also proceeded to construct terraces along the hill, similar to those observed in the ERT profile (Fig. 14a). In this context, the terrace located between the second and

third walls, from bottom to top, placed at 355 m a.s.l., was flattened after a slope scar had already formed. Although terracing is a common technique in geotechnical engineering to enhance slope stability (e.g., Martin Duque et al., et. 2015), it is also frequently employed for agricultural expansion, and erosion control, among other purposes (Wei et al. 2016). Nevertheless, such movements can also increase spatial variability, as well as heterogeneous infiltration and runoff on hillslopes, potentially promoting new slides, particularly in the Mediterranean region, where occasional but intense rainfall events occur (Arnáez et al., 2015). In the case of the Iberian period, terraced settlements was a common technique in urban areas, often associated with defensive purposes.

5.3 Castle levels (XIV-XV centuries) and Ducal granary (XVIII century to present)

After the Iberian period, no clear or just minor evidence of constructions from Imperial Roman (27 BCE to 476 CE), Visigoth (476–711 CE), or Muslim ruling periods has been preserved at Castle Hill, and no landslides have been identified despite significant changes in climate conditions (Fig. 18). The site was either abandoned during this long period or the layers were dismantled during the construction of the fortress when this territory was reclaimed by Christian rulers. A radiocarbon date obtained from the basement offered an age of 1404–1452 cal CE, which aligns with written historical sources (Rey 2017). As previously described, the fortress was demolished in 1508 CE, but its foundations and wall basements were preserved (Figs. 3 and 4, red triangles). Different construction techniques were employed for the fortress, but for this discussion, we will focus on the preserved curtain walls and basements constructed using a rammed-earth technique (Figs. 4 and 19). This technique was widely used in defensive construction during this period (Gutierrez-Carrillo et al. 2021) and involved compacting raw material such as earth, lime, chalk and gravel within a wooden rectangular formwork. When the wood deteriorated, holes were left behind, which can be observed aligned in the walls (Fig. 19).

Originally, these rammed-earth blocks were placed horizontally and without cracks, which allows us to identify different zones of basculation and fracture. The block located northwards was fractured shortly after its construction, as the line of formwork holes is clearly located beneath it and shows the same thickness and layering as the adjacent blocks (Fig. 19a, dashed square). This evidence points that the rammed-earth block was vulnerable to rapid slope movement, likely associated with the plastic deformation of the marls (MS-3,

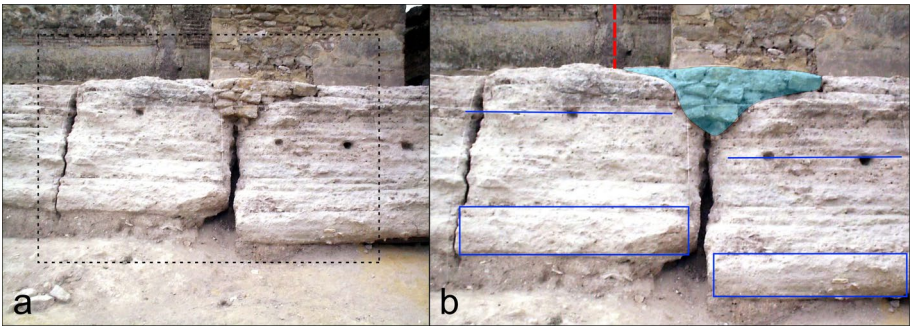

Fig. 19 Detailed photo of the cracking and tilting of the Montilla Castle foundations (XIV-XV centuries) observed in Fig. 4

Fig. 18). This MS-3 potential landslide does not appear to be related to any tsunamigenic event.

The presence of a thin layer of Iberian period wall debris covering the marls may have led the builders to misjudge the soil's bearing capacity. Furthermore, the vertical crack affecting this northern block is located at the boundary between the calcarenite rocks and the marls that composed the hill´s slope, coinciding with the location where our geotechnical model predicts that the circular slip surface would reach the surface (Figs. 9 and 10). Based on these observations, we can infer that the fortress experienced structural stability issues from the outset, particularly concerning the foundations seats on the NW facade. This problem in certain walls was a common issue in castles in the region, which often required periodic reconstructions at gates and walls (e.g., Carmona Castle, Silva et al., 2013). Problems with slope stability may also have contributed to the high demand for repairs (Gallego and Molero García, 2019) and even the eventual abandonment of the Montiel Castle (Ciudad Real, Spain), placed over a steep Triassic clay sequence with abundant evidence of landslides.

As previously described, only the external walls of the fortress were dismantled in 1508 AD. Two years later, the Ducal family was authorized to rebuild the fortress, but in a cryptic decision, they abandoned the keep and other buildings, which were then used as a quarry. Two centuries later, over the ruins, an oversized Ducal granary was constructed in 1722 AD, featuring massive walls, decorative towers and battlements (Fig. 3a and d). Once again, the NW facade of the granary suffered cracks and instabilities (MS-4, Fig. 18), which can be observed both inside (Fig. 20) and outside this building (Fig. 21) including wall repairs. The construction of this massive structure over two distinct geological materials (Fig. 20 left and 21 left) certainly contribute to its structural instability. No historical sources reporting when the NW wall of the Ducal granary was affected by cracks have been found, but it is highly likely that these could be linked to the 1755 Lisbon Earthquake (Mw 8.5). Historical sources describe the effects of this earthquake in Montilla (Martínez Solares, 2001), and it is noted that:

Fig. 20 Image inside the Ducal granary (XVIII century) (Fig. 2–4). It can be observed how granary walls and building foundations are affected by vertical cracks (left), in the landslide crown, with the contact between calcarenites rocks (yellowish color) and marls, along with anthropogenic sediments (grey color). This contact forms a preferential rupture surface that has affected the granary´s flooring (right)

Fig. 21 Image from the Ducal granary (XVIII century). On the left, it is visible how the granary walls were adjusted to the remains of the previous fortress, compensating for earlier movements and surface irregularities and/or wall repairs. On the right, vertical cracks affecting the granary walls are visible

> *"...and in the convents of San Francisco and San Augustin, and in that of San Sebastian the bell tower was ruined, all the houses suffered, and 52 were left uninhabitable."*

In the close town of Montemayor at 12 km, they reported during the shake:

> "*... going out through the Gates they saw falling the walls of a barn that was opposite, and on the other hand detach the shots of the tower that collapsed... the Hermitage of San Sebastian was all destroyed. The water from the fountains was spilled, and that one from the cisterns received a great agitation.*" (Martínez Solares, 2001)

In other towns in the area, Luque at 40 km and Cañete at 50 km, we can read:

> "*In Luque an opening has been made in the earth, and there is another similar one in the next town of Cañete de las Torres*" (Martínez Solares, 2001)

In the studied area, the felt intensity is estimated to have reached a value equal to VII (Martínez Solares, 2001) (Fig. 12). The described hillslope is stable under present-day conditions, but it could be reactivated by an earthquake with this felt intensity, based on seismic modelling, depending on the water saturation conditions (Fig. 11). Additionally, local geological features, such as perched aquifers composed of calcarenites and evaporites over impermeable clays, are known to amplify the effects of an earthquake, as observed in various locations. The local and regional conditions of the Castle Hill are similar to those

Fig. 22 Example of building collapses near the Castle Hill after the 1930 Montilla earthquake

of Carmona Castle (Seville), which was destroyed by an earthquake in 1504 AD (Silva et al., 2013). A similar pattern of castle wall and gates destruction, along with reconstruction events associated with landslides and earthquakes, has been documented at this site (Silva et al., 2009; 2013; Völlmert et al., 2011).

After the 1755 earthquake, a seismic event occurred in AD 1930, known as the "1930 Montilla´s earthquake", with felt intensity equal to VII, as commented above (Carbonell 1930). The available instrumental locations for this earthquake place the epicentre near the studied site (Mezcua and Martínez-Solares, 1983), which align with the occurrence of the largest macroseismic effects. This earthquake resulted in the destruction of over 200 houses (Fig. 22) and affected major buildings in the town, but it was not associated with landslides in the area. The event occurred on 5 July, suggesting that the terrain was likely unsaturated due to the dry season.

6 Summary and conclusions

A multidisciplinary approach combining archaeology, historical archives, electrical resistivity surveys and geotechnical modelling, enabled the reconstruction of Montilla Castle Hill landslides and their impact on human settlements. The instability of the studied site is associate with the presence of perched aquifers, including salt waters, composed of calcarenites and evaporites over impermeable clays with low load-bearing capacity and steep slope.

A long-term interaction between buildings at the studied location and hillslope instabilities has been identified over the past 3,000 yrs. Four phases of landslide activity were observed: MS-1 from 650–550 BCE, MS-2 from 400 to 200 BCE, MS-3 from 1400 to 1450 and MS-4 from the XVIII to the XX century. During the Iberian period (VIII to I century BCE), hillside terracing, following the burning and demolition of constructions, appears to have been the technique used to restore settlement habitability. This technique was applied at least twice, as evidenced by the record. During the Medieval period (XIII to XV centuries), construction pathologies affected the Castle NW facade, related with rapid plastic movements in the marls associated with overpressure. Displaced and fractured rammed-earth blocks were repaired with heightening and new blocks, enabling the creation of a flat surface suitable for construction. In Modern period (XVI to XVIII centuries), the construction of a massive granary promoted new instabilities in the NW façade, similar to those suffered

by the previous fortress. These instabilities appear to be related with the boundary between calcarenites (cohesive rocks) and the soft blue marls, as well as the landslide crown.

Dates based on archaeological remains and absolute radiocarbon analysis indicate that landslides did not show any correlation with climate conditions, but they could be coetaneous with major earthquakes and tsunamigenic events described in other locations in southern Iberia. Specifically, these events include a likely earthquake associate to the "Cerro del Villar tsunami" around 600 BCE, the so-called "Event 5" dated to 330–30 BCE or ~ 218 BCE, and the 1755 Lisbon earthquake. It may not be ruled out that landslides described may also be related to local earthquakes of low to moderate magnitude (5.5–6) that are likely in the area. These findings align with the critical stability threshold value obtained for the building. During the period when the Montilla Castle Hill was unoccupied (from ~ 0 to 1450 CE), landslides do not appear to have been active. This suggests that the presence of major buildings at the summit of Castle Hill, located at the landslide crown, played a key role in promoting the reactivation of ancient landslides.

Acknowledgements The authors appreciate the support and help of Dra. Mara Portero Delgado (architect) and Dr. José Rey (official chronicler of Montilla), Museo Histórico Local de Montilla and Excelentísimo Ayuntamiento de Montilla (Montilla City Council). We also thanks funding from RNM-148 research group of Junta de Andalucía; and BARACA PID2022-136678NB-I00 financed by MICIU/AEI https://doi.org/10.13039/501100011033 and FEDER, UE, and PID2021-125619OB-C21/C22 funded by the Ministerio de Ciencia e Innovación of Spain, the Agencia Estatal de Investigación and the Fondo Europeo de Desarrollo Regional FEDER.

Funding Open Access funding provided thanks to the CRUE-CSIC agreement with Springer Nature. Ministerio de Ciencia, Innovación y Universidades, PID2022-136678NB-I00, Jesús Galindo-Zaldívar, Ministerio de Ciencia e Innovación, PID2021-125619OB-C21/C22, Francisco J. JIMENEZ-ESPEJO

References

Abelleira M, Muñiz I, Roldán A, Caballero A, Pelado I, Adroher AM, Macías I, García A, Moreno D, Matas FJ, Condom J, Fernández JL, Ortiz B, Tinoco L, Mosquera L, Draguet E (2020) La necrópolis de Los Collados de Almedinilla (Córdoba). Historiografía de un cementerio complejo. Antiquitas 32:81–104

Aguirre J, Braga JC, Martín-Pérez JA, Martín JM, Puga-Bernabéu A (2022) Upper Miocene deposits at the southern margin of the Guadalquivir Foreland Basin (central Betic Cordillera, S. Spain). Implications for the closure timing of the Atlantic-Mediterranean connections, Rev. Micropaleontol 76:100690. https://doi.org/10.1016/j.revmic.2022.100690

Alfaro P, Azañón JM, Clavero D, Delgado J, Figueras S, García-Mayordomo J, García-Tortosa FJ, Garrido J, Hernández L, Lenti L, López JA, López Casado C, Macau A, Martino S, Mulas J, Peláez JA, Rodríguez-Peces MJ, Santamarta JC, Silva PG (2021) Seismic induced landslides in Spain: a review. In 7th Conference: Portuguese-Spanish asembly of geodesy and geophysics, donostia-san sebastian. https://doi.org/10.13140/RG.2.1.2213.0801

Álvarez-Martí-Aguilar M, Machuca F (Eds.) (2022a) Hiarchstorical earthquakes, tsunamis and archaeology in the iberian peninsula, Springer, Singapore, https://doi.org/10.1007/978-981-19-1979-4, ISBN 978–981–19–1978–7

Álvarez-Martí-Aguilar M, Suárez-Padilla J, Aubet MA, Machuca F, Martín-Casado JM, Feist L, Val-Peón C, Reicherter K (2022b) Archaeological and geophysical evidence of a high-energy marine event at the phoenician site of cerro del villar (Malaga, Spain), In: historical earthquakes, tsunamis and archaeology in the Iberian Peninsula. Álvarez-Martí-Aguilar M, Machuca Prieto F (eds) Springer, Singapore, 179–201. ISBN 978–981–19–1978–7. https://doi.org/10.1007/978-981-19-1979-4

Álvarez-Martí-Aguilar M (2020) The historicity of the earthquakes occurring in the Iberian Peninsula before A.D. 881 Recorded in Spanish and Portuguese Seismic Catalogs. Seismol Res Let 91:3585–3594. https://doi.org/10.1785/0220200168

Arnaèz J, Lana-Renault N, Lasanta T, Ruiz Flaño P, Castroviejo J (2015) Effects of farming terraces on hydrological and geomorphological processes. A review. CATENA 128:122–134. https://doi.org/10.1016/j.catena.2015.01.021

Bascón JM (2024) Actividad arqueológicapreventiva tipo excavaciónarqueológica en el Castillo del Gran Capitán deMontilla. Expt. AAPRE 154/2022. Arquea 14415. CB 354. Archivo del Ayuntamiento de Montilla y Delegación Territorial de Cultura de Córdoba

Batlló J, Stich D, Macià R, Morales J (2010) Moment tensor inversion for the 5 July 1930 Montilla earthquake (southern Spain). Seismol Res Lett 81(5):724–731. https://doi.org/10.1785/gssrl.81.5.724

Bermúdez Cano JM, Ortiz Urbano R (1999) Informe memoriade la Intervención Arqueológica de Urgencia en el Castillo de Montilla. Administrative report in Delegación Territorial de Cultura, Córdoba, Junta deAndalucía

Bermúdez Cano JMY, Ortiz Urbano R (2001) Las dos Montillas. La ocupación del Cerro del Castillo de Montilla in: Actas de las III Jornadas sobre Historia de Montilla, edited by: Espino Jiménez, F. F. (Ed.), Montilla

Bermúdez Cano JM, Cepillo Galvín JJ, Ortiz Urbano R (2000) Informe de la Intervención Arqueológica de Apoyo a la Restauración del Castillo de Montilla. Administrative report in Delegación Territorial de Cultura, Córdoba, Junta de Andalucía

Bishop AW (1955) The use of the slip circle in the stability analysis of slopes. Geotechnique 5:7–17

Bonet Rosado H (1995) El Tossal de Sant Miquel de Llíria: la antigua Edeta y su territorio. Diputación de Valencia (Ed., Pub.), Paterna, ISBN: 84–7795–981–1

Bronk Ramsey C (2009) Bayesian analysis of radiocarbon dates. Radiocarbon 51(1):337–360. https://doi.org/10.2458/azu_js_rc.51.3494

Buero MS (1988) La cerámica decorada a la almagra del Bronce Final Meridional. Habis 18–19:485–513

Calaforra JM, Pulido-Bosch A (1999) Gypsum karst features as evidence of diapiric processes in the Betic Cordillera, Southern Spain. Geomorphology 29(3–4):251–264. https://doi.org/10.1016/S0169-555X(99)00019-7

Calvo-Serrano MA, Castillejo-González IL, Montes-Tubío F, Mercader-Moyano P (2020) The church tower of Santiago Apóstol in Montilla: an eco-sustainable rehabilitation proposal. Sustainability 12:7104. https://doi.org/10.3390/su12177104

Camuera J, Jiménez-Espejo FJ, Soto-Chica J, Jiménez-Moreno G, García-Alix A, Ramos-Román MJ, Ruha L, Castro-Priego M (2023) Drought as a possible contributor to the Visigothic Kingdom crisis and Islamic expansion in the Iberian Peninsula. Nat Commun 14:5733

Carbonell A (1930) The Montilla earthquake (in Spanish). Boletín De La Cámara Oficial Minera De Córdoba 15:7–10

Carbonell E, Bermúdez de Castro J, Parés J. et al (2008) The first hominin of Europe. Nature 452:465–469, https://doi.org/10.1038/nature06815

Caro Bellido A (1989) Cerámica gris a torno tartesia, Universidad de Cádiz (Ed. Pub.), Cádiz. https://rodin.uca.es/handle/10498/25236

Carrion JS, Fuentes N, González-Sampériz P, Sánchez-Quirante L, Finlayson C, Fernández S, Andrade A (2007) Holocene environmental change in a montane region of southern Europe with a long history of human settlement. Quat Sci Rev 26:1455–1475. https://doi.org/10.1016/j.quascirev.2007.03.013

Delgado J, Peláez JA, Tomas R, García-Torrosa FJ, Alfaro P, López-Casado C (2011a) Seismically-induced landslides in the Betic Cordillera (S Spain). Soil Dyn Earthquake Eng 31:1203–2121

Delgado J, Garrido J, López Casado C, Martino S, Peláez JA (2011b) On far field occurrence of seismically induced landslides. Eng Geol 123:204–213

Escacena Carrasco JL (1987) Cerámicas a torno pintadas andaluzas de la Segunda Edad del Hierro, Ph.D. thesis, University of Seville, http://hdl.handle.net/11441/38404

Escolano F, Bueno M (2015) Stress–strain behaviour of the sediments in the tertiary basins associated with the Alentejo–Plasencia fault in the province of Caceres (Spain). Bull Eng Geol Environ 74(3):733–743. https://doi.org/10.1007/s10064-014-0676-7

Escolano F, Bueno M, Melentijevic S (2019) Stress-strain behavior of blue marls from the Guadalquivir river basin in Spain. Acta Geotech Slov 16(1):30–42. https://doi.org/10.18690/ACTAGEOTECHSLOV.16.1.30-42.2019

Estrada F, González-Vida JM, Peláez JA, Galindo-Zaldívar J, Ortega S, Macías J, Vázquez JT, Ercilla G (2021) Tsunami generation potential of a strike-slip fault tip in the westernmost Mediterranean. Sci Rep 11:16253. https://doi.org/10.1038/s41598-021-95729-6

Everett ME (2013) Near-surface applied geophysics. Cambridge University Press. https://doi.org/10.1017/CBO9781139088435

Fernández T, Pérez-García JL, Gómez-López JM, Cardenal J, Moya F, Delgado J (2021) Multitemporal landslide inventory and activity analysis by means of aerial photogrammetry and LiDAR techniques in an area of Southern Spain. Remote Sens 13(11):2110. https://doi.org/10.3390/rs13112110

Florido Navarro C (1984) Ánforas prerromanas sudibéricas, Habis 15:419–436, ISSN 0210–7694

Gallego D, Molero García JM (2019) La reparación del Castillo de Montiel (Ciudad Real) a través de los mandatos de obra de 1478: estudio documental y material. Actas del Undécimo Congreso Nacional de Historia de la Construcción, Soria 1:469–479. ISBN 978–84–9728–576–6

García Vargas E, Mora de los Reyes M y Ferrer Albelda E (1989) Estudios sobre cerámicas ibéricas andaluzas: Montemolín (Marchena, Sevilla), Habis 20:217–243. ISSN 0210–7694

Gariano SL, Guzzetti F (2016) Landslides in a changing climate. Earth-Sci Rev 162:227–252. https://doi.org/10.1016/j.earscirev.2016.08.011

Gozalbes E (1991) La ciudad antigua de Rusadir: aportaciones a la historia de Melilla en la antigüedad, Servicio de Publicaciones del Excelentísimo Ayuntamiento de Melilla, Melilla ISBN 84–87291–12–0

Gràcia E, Vizcaino A, Escutia C, Asioli A, Rodés A, Pallàs R, García-Orellana J, Lebreiro S, Goldfinger C (2010) Holocene earthquake record offshore Portugal (SW Iberia): testing turbidite paleoseismology in a slow-convergence margin. Quat Sci Rev 29(9–10):1156–1172. https://doi.org/10.1016/J.QUASCIREV.2010.01.010

Guerrero VM (1991) El palacio-santuario de Cancho Roano (Badajoz) y la comercialización de ánforas fenicias indígenas. Rivista di Studi Fenici, XIX, 1:49–82. ISSN 0390–3877

Gutierrez-Carrillo ML, Arizzi A, Bestué Cardiel I, Sebastián Pardo E (2021) Study of the state of conservation and the building materials used in defensive constructions in South-Eastern Spain: the example of Mula Castle in Murcia. Int J Architect Herit 15(4):567–579. https://doi.org/10.1080/15583058.2019.1630516

Haque U, da Silva PF, Devoli G, Pilz J, Zhao B, Khaloua A, Wilopo W, Andersen P, Lu P, Lee J, Yamamoto T, Keellings D, Wu J-H, Glass GE (2019) The human cost of global warming: deadly landslides and their triggers (1995–2014). Sci Total Environ 682:673–684. https://doi.org/10.1016/j.scitotenv.2019.03.415

Henares J, López Casado C, de Sanz Galeano C, Delgado J, Peláez JA (2003) Stress fields in the Iberian-Maghrebi region. J Seismol 7:65–78. https://doi.org/10.1023/A:1021294015027

Highland LM, Bobrowsky P (2008) The landslide handbook-a guide to understanding landslides (No. 1325). US Geological Survey ISBN: 978–141132226–4

Hungr O, Leroueil S, Picarelli L (2014) The varnes classification of landslide types, an update. Landslides 11:167–194. https://doi.org/10.1007/s10346-013-0436-y

Jabalquinto, IM, Bascón, JM, Del Pino, J (2013) Informe de la Intervención Arqueológica de la actividad arqueológica preventiva desarrollada en la senda peatonal del castillo de Montilla. Administrative report in Delegación Territorial de Cultura, Córdoba, Junta de Andalucía.

Jabalquinto IM, Bascón JM, Del Pino J (2020) Los orígenes de la localidad de Montilla (Córdoba) a través de los resultados obtenidos de la actividad arqueológica preventiva desarrollada en la senda peatonal del castillo, http://hdl.handle.net/20.500.11947/26065, 2020.

Janbu N, Bjerrum L, Kjarnsli B (1956) Stabilitetsberegning for fyllinger skjaeringer og naturlige skraninger. Norwergian Geotech. Public 16

Jiménez-Espejo FJ, López-Sáez JA, Bulian F, Valiente S, Giles F, Ayarzagüena Sanz M, Garrido-Pena R, Gonzalez-Ramón A, Carrascal JM, López Cidad F, Barril Vicente M, Camuera J (2024) Salt production by ignition during the prehistory in the Iberian Peninsula with special focus on the archaeological site of Espartinas (Ciempozuelos, Spain). Quat Sci Rev 336:108775. https://doi.org/10.1016/j.quascirev.2024.108775

Kárník V (1969) Seismicity of the European Area, Part 1, Reidel, Dodrecht, Netherlands, ISBN: 978–9027701213

Ladrón de Guevara I (1994) Aportación al estudio de la cerámica con impresiones digitales en Andalucía, Servicio de Publicaciones de la Universidad de Cádiz, http://hdl.handle.net/10498/26193

Lario J, Zazo C, Goy JL, Silva PG, Bardaji T, Cabero A, Dabrio CJ (2011) Holocene paleotsunami catalogue of SW Iberia. Quat Int 242(1):196–200. https://doi.org/10.1016/j.quaint.2011.01.036

Lenti L, Martino S, Delgado J, Galiana JJ, López Casado C, Garrido J, Sanz de Galdeano C, Peláez JA, García Tortosa FJ (2016) Seismic response of the Güevéjar landslide (S Spain), In: Landslides and engineered slopes, theory and practice. Aversa S, Cascini L, Picarelli L, Scavia C (eds) CRC Press, London, 1259–1266. https://doi.org/10.1201/b21520-153

López Rodríguez R (2010) Memoria Preliminar de la Actividad Arqueológica Puntual: Ordenación del Reciento del Castillo y Restauración del Alhorí, Montilla (2ª Fase). Delegación Provincial de Cultura Córdoba

Luque L, Lario J, Zazo C, Goy JL, Dabrio CJ, Silva PG (2001) Tsunami deposits as paleoseismic indicators: examples from the Spanish coast. Acta Geol Hisp 36(3–4):197–211

Marescot L, Loke MH, Chapellier D, Delaloye R, Lambiel C, Reynard E (2003) Assessing reliability of 2D resistivity imaging in mountain permafrost studies using the depth of investigation index method. Near Surf Geophys 1(2):57–67. https://doi.org/10.3997/1873-0604.2002007

Martín Duque F, Zapico I, Oyarzun R, López García JA, Cubas P (2015) A descriptive and quantitative approach regarding erosion and development of landforms on abandoned mine tailings: new insights and environmental implications from SE Spain. J Geomorphol 239:1–16

Martínez Solares JM (2001) Los efectos en España del terremoto de Lisboa (1 noviembre de 1755), Monografía 19, Instituto Geográfico Nacional, Madrid, ISBN: 84–95.172–26–7

Martínez-Moreno FJ, Pedrera A, Ruano P, Galindo-Zaldívar J, Martos-Rosillo S, González-Castillo L, Sánchez-Úbeda JP, Marín-Lechado C (2013) Combined microgravity, electrical resistivity tomography and induced polarization to detect deeply buried caves: Algaidilla cave (Southern Spain). Eng Geol 162:67–78. https://doi.org/10.1016/j.enggeo.2013.05.008

Martínez-Moreno FJ, Monteiro-Santos FA, Bernardo I, Farzamian M, Nascimento C, Fernandes J, Casal S, Ribeiro JA (2017) Identifying seawater intrusion in coastal areas by means of 1D and quasi-2D joint inversion of TDEM and VES data. J Hydrol 552:609–619. https://doi.org/10.1016/j.jhydrol.2017.07.026

Martínez-Moreno FJ, Delgado-Ramos F, Galindo-Zaldívar J, Martín-Rosales W, López-Chicano M, González-Castillo L (2018) Identification of leakage and potential areas for internal erosion combining ERT and IP techniques at the Negratín Dam left abutment (Granada, southern Spain). Eng Geol 240:74–80. https://doi.org/10.1016/j.enggeo.2018.04.012

Martos-Rosillo S, Ruiz-Constán A, González-Ramón A, Mediavilla R, Martín-Civantos JM, Martínez-Moreno FJ, Jódar J, Marín-Lechado C, Medialdea A, Galindo-Zaldívar J, Pedrera A, Durán JJ (2019) The oldest managed aquifer recharge system in Europe: new insights from the Espino recharge channel (Sierra Nevada, southern Spain). J Hydrol 578:124047. https://doi.org/10.1016/j.jhydrol.2019.124047

Merritt AJ, Chambers JE, Murphy W, Wilkinson PB, West LJ, Uhlemann S, Meldrum PI, Gunn D (2018) Landslide activation behaviour illuminated by electrical resistance monitoring. Earth Surf Process Landforms 43(6):1321–1334. https://doi.org/10.1002/esp.4316

Mezcua J, Martínez JM (1983) Sismicidad del área Ibero-mogrebi. Publicación 203, Instituto Geográfico Nacional, Madrid

Milo P, Vágner M, Tencer T, Murín I (2022) Application of geophysical methods in archaeological survey of early medieval fortifications. Remote Sens 14(10):2471. https://doi.org/10.3390/rs14102471

Morgenstein NR, Price VE (1965) The analysis of the stability of general slip surfaces. Geotech 15:70–93

Murillo JF (1994) La Cultura Tartésica en el Guadalquivir Medio, Ariadna, 13–14, Excmo. Ayuntamiento de Palma del Río, Palma del Río, ISSN 1130–8141

NCSE-02 (2002) Norma de construcción sismoresistente parte general y edificación. Real Decreto 977/2002, 27-Sep, del Ministerio de Obras Públicas, Transportes y Medio Ambiente. B.O.E. 8-Feb-95

Negueruela I (1980) Sobre la cerámica de engobe rojo en España, Habis, 10–11, 335–359, ISSN 0210–7694

Noel M, Xu B (1991) Archaeological investigation by electrical resistivity tomography: a preliminary study. Geophys J Int 107(1):95–102

Ocampo F (1553) de: Los Cinco Libros Primeros de la Crónica General de España, que Recopila el Maestro Florian do Campo, Cronista del Rey Nuestro Señor, Guillermo de Millis, Medina del Campo, Spain. https://www.cervantesvirtual.com/obra/los-cinco-libros-primeros-de-la-cronica-general-de-espana/

Oliveira CS (2008) Review of the 1755 lisbon earthquake based on recent analyses of historical observations. In: Historical Seismology. Frechet J, Meghraoui M, Stucchi M (eds) Springer. https://doi.org/10.1007/978-1-4020-8222-1_13

Ortiz R (2018) Protohistoria en la campiña de Córdoba. Análisis arqueológico de la secuencia estratigráfica del Castillo de Montilla. Ph.D. Thesis, Univ. de Córdoba. Dra. María Belén Deamos Ph.D. advisor

Outiskt M, Tadibaght A, Agharroud K, Baptista MA, Francisco PRJ, Tichli S, Aboumaria K (2025) Quantitative risk assessment of a tsunami induced by the Averroes Fault (Alboran Sea): case of Martil City, the Mediterranean coast of Morocco. Pure Appl Geophys 182:311–331. https://doi.org/10.1007/s00024-025-03681-7

Papadopoulos N, Sarris A, Yi MJ, Kim JH (2009) Urban archaeological investigations using surface 3D ground penetrating radar and electrical resistivity tomography methods. Explor Geophys 40(1):56–68. https://doi.org/10.1071/EG08107

Pellicer Catalán M (1978) Tipología y cronología de las ánforas prerromanas del Guadalquivir según el Cerro Macareno (Sevilla), Habis, 9: 365–400, ISSN 0210–7694

Pereira J (1988b) La cerámica ibérica de la Cuenca del Guadalquivir. I. Propuesta de Clasificación. Trab Prehist 45:143–173. https://doi.org/10.3989/tp.1988.v45.i0.608
Pereira J (1989) La cerámica ibérica de la Cuenca del Guadalquivir. II. Conclusiones. Trab Prehist 46:149–159. https://doi.org/10.3989/tp.1989.v46.i0.592
Pereira J (1988a) La cerámica pintada a torno en Andalucía entre los siglos VI y III a.d.C. Cuenca del Guadalquivir, Ph.D. thesis, nº 406/88. Universidad Complutense, Madrid
Pérez-Valera F, Sánchez-Gómez M, Pérez-López A, Pérez-Valera LA (2017) An evaporite-bearing accretionary complex in the northern front of the Betic-Rif orogen. Tectonics 36(6):1006–1036. https://doi.org/10.1002/2016TC004414
Portero Delgado MA (2020) Estimate of the virtual reconstruction of the castle of montilla. Ph. D. Tesis. University of Córdoba, Spain. https://helvia.uco.es/xmlui/handle/10396/20354
Ramón Torres J (1995) Las Ánforas fenicio-púnicas del Mediterráneo central y occidental, Col. Instrumenta, 2, Publicacions Universitat de Barcelona, ISBN 84–475–0992–3
Reimer PJ, Austin WEN, Bard E, Bayliss A, Blackwell PG, Bronk Ramsey C, Butzin M, Cheng H, Edwards RL, Friedrich M, Grootes PM, Guilderson TP, Hajdas I, Heaton TJ, Hogg AG, Hughen KA, Kromer B, Manning SW, Muscheler R, Palmer JG, Pearson C, van der Plicht J, Reimer RW, Richards DA, Scott EM, Southon JR, Turney CSM, Wacker L, Adolphi F, Büntgen U, Capano M, Fahrni SM, Fogtmann-Schulz A, Friedrich R, Köhler P, Kudsk S, Miyake F, Olsen J, Reinig F, Sakamoto M, Sookdeo A, Talamo S (2020) The IntCal20 Northern Hemisphere radiocarbon age calibration curve (0–55 cal kBP). Radiocarbon 62(4):725–757. https://doi.org/10.1017/RDC.2020.41
Rey J (2017) El Castillo y la Villa medieval de Montilla, ISBN: CO 1913–2017
Reynolds JM (2011) An Introduction to Applied and Environmental Geophysics, 2nd ed, Wiley, Hoboken, ISBN 978-0-471-48535-3
Rodríguez-Vidal J, Ruiz F, Cáceres LM, Abad ML, González-Regalado, Pozo M, Carretero MI, Monge AM, Gómez F (2011) Geomarkers of the 218–209 BC Atlantic tsunami in the Roman Lacus Ligustinus (SW Spain): a palaeogeographical approach, Quat. Int 242:201–212, https://ui.adsabs.harvard.edu/link_gateway/2011QuInt.242..201R/. https://doi.org/10.1016/j.quaint.2011.01.032
Roldán García FJ, Divar Rodríguez J, García Cortés A (1985) Mapa geológico y Memoria de la Hoja nº 966 (16–39) Montilla. Mapa Geológico de España E. 1:200.000, IGME
Roos AM (1982) Acerca de la antigua cerámica gris a torno en la Península Ibérica. Ampurias 44:43–70
Rufete P (1989) La cerámica con barniz rojo de Huelva, in: Tartessos, Arqueología Protohistórica del Bajo Guadalquivir, edited by: Aubet, M.A., AUSA, 375–394, ISBN: 84–86329–48–5
Ruiz F, Rodríguez-Vidal J, Abad M, Cáceres LM, Carretero MI, Pozo M, Rodríguez-Llanes JM, Gómez-Toscano F, Izquierdo T, Font E, Toscano A (2013) Sedimentological and geomorphological imprints of Holocene tsunamis in southwestern Spain: an approach to establish the recurrence period. Geomorphology 203:97–104. https://doi.org/10.1016/j.geomorph.2013.09.008
Ruiz Mata D (1995) Las cerámicas del Bronce Final. Un soporte tipológico para delimitar el tiempo y el espacio tartésico. In: Tartessos, 25 años después. 1968–1993. Ayuntamiento de Jerez de la Frontera (eds). Actas del Congreso Conmemorativo del V Symposium Internacional de Prehistoria Peninsular, 265–313, ISBN: 84–87194–64–8
Sanz E (1997) Le mouvement de versant de Güevéjar (Grenade) au cours des tremblements de terre de Lisbonne (1755) et d'Andalousie (1884). Bull Int Assoc Eng Geol 56:83–87
Sassa K, Mikoš M, Yin Y (2017) Advancing culture of living with landslides. WLF 2017. Springer, Cham. https://doi.org/10.1007/978-3-319-59469-9
Scawthorn C, Nishino T, Schenking C, Borland J (2023) Kantō Daikasai: The Great Kantō Fire Following the 1923 Earthquake. Bull Seism Soc Amer 113:1902–1903
Sekizawa A (2023) 1923 great Kanto earthquake: fire damage and lessons learned. J Disast Res 18:558–561
Silva PG, Rodríguez-Pascua MA, Pérez-López R, Giner-Robles JL, Lario J, Bardají T, Goy JL, Zazo C (2009) Geological and archaeological record of the 1504 AD Carmona earthquake (Guadalquivir Basin, SouthSpain): a review after Bonsor, 1918. In: Archaeoseismology and palaeoseismology in the alpine-himalayan collisional zone. Pérez-López R, Grützner C, Lario J, Reicherter K, Silva PG (eds) 1st INQUA-IGCP 567 International workshop on earthquake archaeology and palaeoseismology, Baelo Claudia, Spain, 139–142
Silva PG, Rodríguez-Pascua MA, Giner Robles JL, Pérez López R, Reicherter K, Bardají T, Goy JL, Zazo C (2013) Efectos geológicos y arqueológicos producidos por el terremoto de Carmona de 1504 AD (Cuenca del Guadalquivir, sur España) Datos preliminares sobre las posibles fuentes sísmicas, Cuaternario y geomorfología: Revista de la Sociedad Española de Geomorfología y Asociación Española para el Estudio del Cuaternario, 27, 109–125, ISSN 0214–1744
Sparacino F, Palano M, Peláez JA, Fernández J (2020) Geodetic deformation versus seismic crustal moment-rates: insights from the Ibero-Maghrebian region. Remote Sens 12:952. https://doi.org/10.3390/rs12060952

Spencer E (1967) A method of analysis of the stability of embankments assuming parallel inter-slice forces. Géotechnique 17:11–26

Svennevig K, Koch J, Keiding M, Luetzenburg G (2024) Assessing the impact of climate change on landslides near Vejle, Denmark, using public data. Nat Hazards Earth Syst Sci 24:1897–1911. https://doi.org/10.5194/nhess-24-1897-2024

Telford WM, Geldart LP, Sheriff RE (1990) Applied geophysics, 2nd ed. Cambridge University Press, Cambridge. ISBN 978-0-521-32693-3

Uhlemann S, Kuras O, Richards LA, Naden E, Polya DA (2017) Electrical resistivity tomography determines the spatial distribution of clay layer thickness and aquifer vulnerability, Kandal Province, Cambodia. J Asian Earth Sci 147:402–414. https://doi.org/10.1016/j.jseaes.2017.07.043

Vaquerizo Gil D, Quesada Sanz F, Murillo Redondo JF (1992) La cerámica ibérica del Cerro de la Cruz (Almedinilla, Córdoba). Departamentos O, P, Ñ. An Arqueol Cordob 3:51–112

Vázquez JT, Ercilla G, Alonso B, Peláez JA., Palomino D, León R, Bárcenas P, Casas D, Estrada F, Fernández Puga MC, Galindo Zaldívar J, Henares J, Llorente M, Sánchez, Guillamón O, d'Acremont E, Ammar A, Chourak M, Fernández Salas LM, López González N, Lafuerza S (2022) Triggering mechanisms of tsunamis in the gulf of cadiz and the Alboran Sea: an overview. In: historical earthquakes, tsunamis and archaeology in the Iberian Peninsula. Natural Science in Archaeology. Álvarez-Martí-Aguilar M, Machuca Prieto F (eds) Springer, Singapore, 65–104. https://doi.org/10.1007/978-981-19-1979-4_8

Vázquez-Boza M, Justo JL, Durand P, Morales-Esteban A (2014) Macro and microstructure of Guadalquivir blue marls in cyclic suction-controlled drying and wetting test. In: Unsaturated Soils: Research & Application, 1st ed. CRC Press. https://doi.org/10.1201/9781003070580

De Vicente, G, Cloetingh S, Muñoz-Martín A, Olaiz A, Stich D, Vegas R, Galindo-Zaldívar J, Fernández-Lozano J (2008) Inversion of moment tensor focal mechanisms for active stresses around the microcontinent Iberia: Tectonic implications. Tectonics. 27. https://doi.org/10.1029/2006TC002093

Völlmert A, Reicherter K, Silva PG, Fernandez-Steeger TM (2011) Landslide mapping to analyse earthquake environmental effects (EEE) in Carmona, Spain–Relation to the 1504 event. 2nd INQUA-IGCP-567 International workshop on active tectonics, earthquake geology, archaeology and engineering, Corinth, Greece.

Wei W, Chen D, Wang L, Daryanto S, Chen L, Yu Y, Lu Y, Sun G, Feng T (2016) Global synthesis of the classifications, distributions, benefits and issues of terracing. Earth-Sci Rev 159:388–403. https://doi.org/10.1016/j.earscirev.2016.06.010

Whiteley S, Chambers JE, Uhlemann S, Wilkinson PB, Kendall JM (2019) Geophysical monitoring of moisture-induced landslides: a review. Rev Geophys 57(1):106–145. https://doi.org/10.1029/2018RG000603

Whiteley JS, Watlet A, Uhlemann S, Wilkinson P, Boyd JP, Jordan C, Kendall JM, Chambers JE (2021) Rapid characterisation of landslide heterogeneity using unsupervised classification of electrical resistivity and seismic refraction surveys. Eng Geol 290:106189. https://doi.org/10.1016/j.enggeo.2021.106189

Authors and Affiliations

Francisco J. Jiménez-Espejo[1] · Lourdes González-Castillo[2] · Francisco Lamas[3] · Francisco José Martínez-Moreno[4] · Jesús Galindo-Zaldívar[2,5] · Jon Camuera[6] · Sergio Moyano[7] · José A. Peláez[8] · José Luis Urbano[7] · Mónica Camacho Calderón[9] · Raimundo Ortiz[10]

✉ Francisco J. Jiménez-Espejo
francisco.jimenez@csic.es

[1] Instituto Andaluz de Ciencias de La Tierra (CSIC), 18100 Armilla, Spain

[2] Departamento de Geodinámica, Universidad de Granada, Granada, Spain

[3] E.T.S. de Arquitectura, Universidad de Granada, Granada, Spain

[4] Departamento de Geodinámica, Estratigrafía y Paleontología, Universidad Complutense de Madrid, Madrid, Spain

[5] Instituto Andaluz de Ciencias de La Tierra (UGR), Granada, Spain

[6] Unidad de Botánica, Facultad de Farmacia, Universidad Complutense de Madrid, Madrid, Spain

[7] Museo Histórico Local de Montilla, Montilla, Spain

[8] Departamento de Física, Universidad de Jaén, Jaén, Spain

[9] Departamento de Prehistoria y Arqueología, Universidad Autónoma de Madrid, Madrid, Spain

[10] Cabildo Catedral de Córdoba, Arqueólogo, Córdoba, Spain